UNIVERSITY OF GHANA

COLLEGE OF BASIC AND APPLIED SCIENCE

BIOSYNTHESIS OF MAGNETIC IRON OXIDE NANOPARTICLES AND ITS POTENTIAL APPLICATION IN CANCER TREATMENT.

BY

NII AMARKAI AMARTEY

(10388154)

A THESIS SUBMITTED TO THE SCHOOL OF GRADUATE STUDIES IN PARTIAL FULFILMENT OF THE AWARD OF DEGREE OF MASTER OF PHILOSOPHY IN MATERIALS SCIENCE AND ENGINEERING

DEPARTMENT OF MATERIALS SCIENCE AND ENGINEERING

2018

UNIVERSITY OF GHANA

COLLEGE OF BASIC AND APPLIED SCIENCE

BIOSYNTHESIS OF MAGNETIC IRON OXIDE NANOPARTICLES AND ITS POTENTIAL APPLICATION IN CANCER TREATMENT.

BY

NII AMARKAI AMARTEY

(10388154)

A THESIS SUBMITTED TO THE SCHOOL OF GRADUATE STUDIES IN PARTIAL FULFILMENT OF THE AWARD OF DEGREE OF MASTER OF PHILOSOPHY IN MATERIALS SCIENCE AND ENGINEERING

DEPARTMENT OF MATERIALS SCIENCE AND ENGINEERING

2018

DECLARATION

Candidate's Declaration

I hereby declare that this MPhil thesis which is the result of my own original research under strict supervision was prepared in accordance with the University of Ghana's academic regulations and that no part of it has been presented for another degree in this University or elsewhere.

Candidates' name: Nii Amarkai Amartey

Signature:…… Date:……

Supervisor's Declaration

We hereby declare that the presentation and presentation of this MPhil thesis were supervised in accordance with the guidelines on supervision of MPhil these laid down by the University of Ghana.

Supervisor: Dr. Johnson Efavi

Signature:…… Date:……

Co-Supervisor: Dr. Elvis K. Tiburu

Signature:…… Date:……

Head of Department's Declaration

I hereby declare that this MPhil these has been prepared supervised and accepted in accordance with the guidelines on the MPhil thesis laid down by the University of Ghana

Head of Departments: Dr. Lucas Nana Wiredu Damoah

Signature:…… Date:……

ABSTRACT

Cancer is one of the leading causes of death globally and its treatment and cure are therefore very important. Chemotherapy, radiation, and surgery have been the major forms of treatment. In this work, magnetic Fe_3O_4 nanoparticles are biologically synthesized using maize leaves, plantain leaves and peels extracts as mediators. The synthesized particles were magnetic and this aided in their washing after the synthesis. UV-Vis spectroscopy pointed to the formation of the Fe_3O_4 nanoparticles as the absorption wavelength range of 300-800 nm was recorded. EDX data obtained showed the presence of Fe and O, depicting the presence of iron oxide in the sample. The EDX data also showed the presence of other elements such as Ca and K which were considered an evidence of the complexity of the plant extracts employed in the synthesis. FTIR analysis was conducted for both the plants used and the particles synthesized. The spectra, which was between ~3500 – ~450 cm^{-1}, pointed to the presence of phenol compounds and proteins in the plant extracts that contributed to the formation of the magnetic Fe_3O_4 nanoparticles. It also showed the presence of Fe-O bonds at a wavenumber of 544 cm^{-1}. SEM images obtained showed varying levels of agglomeration in particles formed. The particles were used on Hela cell and recorded a reduction in cell viability. The particles were responsible for a reduction of the cell viability (50.41- 60.82).

DEDICATION

This work is dedicated to my parents, The Late Rev. George Merc Amartey and Mrs. Judith Amartey for their unwavering support throughout my education.

ACKNOWLEDGEMENTS

First of all, I thank the Lord Almighty for the gift of life and good health throughout my study. A special thanks also go to my Supervisors, Dr. Johnson Efavi and Dr. Elvis K. Tiburu for their advice, and directions throughout this work.

I will also like to thank, Dr. Emmanuel Nyankson, Dr. Benjamin Agyei-Tuffour, Dr. Abu Yaya, Dr. David Dodoo-Arhin, Dr. Lucas N. W. Damoah and Dr. Yaw Delali Bensah and Prof. B. Onwona-Agyeman, for all their advice and encouragements during my time of the study.

Table of Contents

LIST OF TABLES

LIST OF FIGURES

LIST OF ABBREVIATIONS

ABBREVIATIONS	FULL MEANING
Fe	Iron
Fe_3O_4	Iron Oxide
Fe_2O_3	Magnesium
NPs	Nanoparticles
OH	Hydroxide
IONPs	Iron Oxide Nanoparticles
pH	Potential Hydrogen
NaOH	Sodium Hydroxide
CN	Cyanide
CO	Carbon dioxide
B-CLL	B-Cell Chronic Lymphocytic Leukemia
IAP	Inhibitor of apoptosis
EGCG	Epigallocatechin-Gallate
SEM	Scanning Electron Microscopy
XRD	X-Ray Diffraction
FDA	Food and Drugs Administration
MM	Multiple myelomas
$FeCl_2$	Iron(II) chloride

$FeCl_3$	Iron(III) chloride
PP-FePs	Plantain Peels Iron Oxide Nanoparticles
PL-FePs	Plantain Leaves Iron Oxide Nanoparticles
ML-FePs	Maize Leaves Iron Oxide Nanoparticles
ROS	Reactive oxygen species
K	Potassium
Ca	Calcium
Mn	Magnesium
MRI	Magnetic Resonance Imaging
CV	Cyclic Voltammetry
EDX	Energy -Dispersive X-Ray Spectroscopy

CHAPTER ONE

1.0. INTRODUCTION

Cancer occurs when unhealthy cells undergo uncontrollable cell division. These cells spread quickly, invading and affecting healthy cells at other parts of the body. Due to the nature of this disease, it has emerged as one with high mortality globally in the healthcare sector and the main cause of 7.8 million deaths in 2008 [1]. Even though many attempts are being made to reduce its quickly rising mortality rate, the major challenge in this agenda is in its prevention and early treatment, since full recovery and reduction in deaths associated with many types of cancers can be increased by early detection and diagnosis [1, 2].

Nanomedicine has emerged as a potential solution in the remediation of cancer, with the introduction of nanoscale materials capable of imaging and detection of cancers. The control over these particles during their application in cancer treatment has led to research into magnetic nanoparticles (NPs) which can be controlled using their magnetic properties. These magnetic nanoparticles in their applications have usually composed a magnetic core engulfed with various functional groups aiding them in hyperthermia treatment, magnetic resonance imaging (MRI), optical imaging, biosensor, cell separation etc. [3-9]. These magnetic nanoparticles in cancer treatment can be directed to particular cancer sites for drug delivery using external magnetics. Also, in the detection of cancer growth, they can be scanned with MRI's when developed and designed by embedding them with receptors that are attracted to cancer cell.

In this field of cancer treatment using magnetic nanoparticles, various researches have focused on magnetic Fe_3O_4 NPs owing to their non-toxicity [5], size variations as well as superparamagnetic properties. Synthesized Fe_3O_4 NPs smaller than biological entities can be coated with different types of organic and inorganic molecules and dispersed in the fluid to

form magnetic fluids These magnetic fluids can be employed in the delivery of targeted drugs such as anticancer drugs [10-12]. In anticancer drugs delivery, magnetic Fe_3O_4 have been engineered to delivery drugs even in response to magnetic signals (magnetically responsive drug delivery therapy) [13, 14]. They are not only employed in drug delivery, tissue repairs, Magnetic resonance imaging (MRI), cell labeling, hyperthermia and detoxification of biological fluids are few other ways in which they have been employed in cancer treatment.

Literature has revealed several methods employed in the synthesizing these of Fe_3O_4 magnetic nanoparticles. Some of these include forced hydrolysis, hydrothermal technique, microemulsion method, sol-gel method, template synthesis among others. The co-precipitation synthesis approach is the simplest and most efficient method among many reported [9, 15-18]. However, these chemical methods, though produce large particles of nanoparticles bearing controlled size and shape within a short time, are expensive, outdated hazardous and complicated. They use chemicals that yield high amounts of hazardous and toxic waste materials.

The biological synthesis approach is another important synthesis method. This method of synthesizing Fe_3O_4 magnetic nanoparticles greatly reduces all forms of environmental hazards by the employment of biological materials and organisms which include algae, bacteria, actinomycetes, yeast, fungi and plants (biological resources) [18]. According to recent studies, synthesizing Fe_3O_4 NPs using non-toxic biocompatible materials at ambient conditions produce clean, eco-friendly and cost-effective nanoparticles. Most successful biosynthesis of stable magnetic nanoparticles employ strong stabilization agents which prevent the agglomeration of nanoparticles providing stability of the Nano system [18, 19]. These stabilization agents include proteins, other biomolecules as well as secondary metabolites which are naturally found in the biological resources used [20].

A widespread of biological resources like microorganisms and plants can be employed in nanoparticle synthesis [21]. Plant extracts are capable of reducing metal ions quicker compared to microbes [21]. Depending on the plant type and phytochemicals present in the plants, the nanoparticles are synthesized in few minutes or hours, whereas microorganism-mediated methods require a longer time [22]. These reasons and the easy availability of plants in nature, make plants favorable biological resources than microbes. These plants naturally come equipped with reducing agents that reduced inorganic iron salts employed in the synthesizing of the Fe_3O_4 nanoparticles as well as stabilizing the particles.

1.1. Problem Statement

Cancer has become a great predicament in the healthcare delivery sector due to its rapid emergence as a high cause of increase in mortality worldwide. Even though great efforts have been made towards its treatment and remediation, there still remain significant room for improvement. The growing age of nanotechnology offers improvement in cancer therapy due to the introduction of magnetic nanoparticles. Fe_3O_4 nanoparticles have been narrowed on as a viable probe in the detecting, targeting and treatment of cancer in addition to the pre-existing 3 major cancer treatment methods. However, the production and synthesis of Fe_3O_4 may require the use of several reported approaches many of which employ the use of expensive yet toxic chemicals which lead to the formation of hazardous by-products and contamination from precursor chemicals used. Also, in order to increase biocompatibility and reduce the toxicity of these Fe_3O_4 nanoparticles produced via these chemical approaches during the treatment of cancer, additional treatments of these nanoparticles become very necessary which again results in the increase in the cost of production of the nanoparticles.

1.2. Research Justification

The research into various way of treating cancer is speedily ongoing. Numerous researches have centered on the use of magnetic iron oxide nanoparticles among other reported means of treatment. In the production of this metal oxide, many approaches have been reported but already existing cancer treatment approaches are known to be very expensive, hence methods to be employed in producing these magnetic oxides must be cost-efficient. The chemical approaches reported by many literatures are very effective in producing these magnetic iron oxides but come at a great cost owing to the cost of chemicals employed. Another approach gaining ground gradually is the biosynthesis approach which is quite cost-efficient and environmentally friendly due to the employment of biological sources found in our very surrounding. The ease of obtaining plant sources, as an example of these biological sources, has led to the development of the green synthesis approach where green plants are employed as mediators (reducing, capping and stabilizing agents), in the synthesis of these iron oxide nanoparticles.

1.3. Aims and Objectives

This work seeks to produce Fe_3O_4 nanoparticles using the green synthesis approach for application in health care delivery

To achieve the above, the following objects will be undertaken;

- Synthesis of magnetic iron oxide Fe_3O_4 nanoparticles using extracts of maize blade leaves, plantain leaves and peels.
- Determining the effect of the synthesis process on the texture of the nanoparticles produced.
- Test the therapeutic effect of the nanoparticles of the nanoparticles on cancer cell.

1.4. Research Question and Hypothesis

1.4.1. Research Question

i. Can plant extracts from maize leaves, plantain peels and leaves reduced iron chloride solution to produce to produce Fe_3O_4 nanoparticles?

ii. Does the concentration and molar ratios of the precursors used affect the morphology of the Fe_3O_4 nanoparticles produced?

iii. Is there an effect of the Fe_3O_4 nanoparticles produced on cancer cells?

iv. Are the effects of the Fe_3O_4 on cancer cells affected by the morphology of the nanoparticles?

1.4.2. Hypothesis

Magnetic Fe_3O_4 nanoparticles have been produced by the reduction of iron chloride in many reported approaches. Chemical reducing agents (such as Sodium boro-hydrate NaBH4) and stabilizing agents have been employed in synthesizing them under the chemical method. When synthesized and functionalized, they have shown potential uses in cancer treatment. Plants extracts, on the other hand, have been reported to be rich in diverse metabolites or biomolecules which have reducing and stabilizing capabilities when reacted with inorganic compounds. Some of these metabolites and biomolecules possess cancer inhibition capabilities.

We, therefore, hypothesize that the extract of maize leaves, plantain leaves and peels, when reacted with iron chloride solution, at varying concentrations, can lead to the production of Fe_3O_4 nanoparticles that have therapeutic effects on cancer cells.

1.5. Scope and Limitation

1.5.1. Scope

This research focused on applying the green synthesis approach using 3 plant extracts, thus maize leaves, plantain peels and plantain leaves. The research is limited to these plants and for checking the effect on only one type of cancer cells.

1.5.2. Limitation

The study was limited in the following ways:

i. The nanoparticles were tried only on one cancer cell.

ii. The effect of the volume of the extracts used was not considered in this study.

CHAPTER TWO

2.0. LITERATURE REVIEW

Iron Oxides exist in different forms but commonly spoken of are three main types which include magnetite, maghemite, and hematite. Their individual atomic structures affect their magnetism (thus: antiferromagnetic, Ferromagnetic and Ferromagnetic properties). The common magnetic iron oxide (i.e. Magnetite) can be synthesized using many approaches which include the co-precipitation approach, thermal decomposition approach, solvothermal and hydrothermal approaches, sonochemical approach and biological approaches. Each process has important advantages and disadvantages affecting their selection in producing specific iron oxide nanoparticles. In order to achieve biocompatibility in relation to the area of application, the biological approach is preferred in the research.

This section, therefore, reviews published literature on Iron Oxide Nanoparticles, their synthesis, their effect on cancer cells (biomedical applications).

2.1. Iron Oxide

Iron oxides are naturally found in eight forms with the commonest being magnetite (Fe_3O_4), maghemite (γ- Fe_2O_3), and hematite (α- Fe_2O_3) [23]. They each have unique catalytic, magnetic, biochemical, physical and many other properties making them suitable for special biomedical applications. The table below Table 2.1 shows their magnetic and physical properties.

These three iron oxides have crystal structures which can be described with respect to planes of iron cations and oxygen anions in close-packed tetrahedral or octahedral interstitial sites [23].

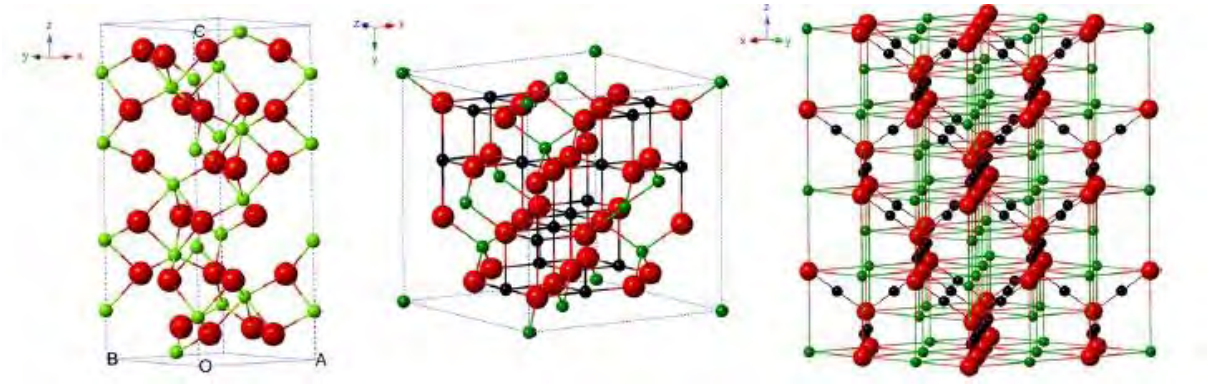

Figure 2. 1 Crystal Structures of Iron Oxides [24]. (a) Hematite (b) Magnetite (c) Maghemite

2.1.1. Hematite (α- Fe_2O_3)

The most stable form of iron oxide is Hematite, found in large amounts in soils and rocks. Hematite possesses high corrosion resistance and is relatively cheap. As a result, it is extensively employed gas sensors, catalysts and pigment. At ambient conditions, it exists as an n-type semiconductor with extremely good stability. In the synthesis of the maghemite and magnetite, it can serve as the starting material [25]. It has various names which include ferric oxide, kidney ore and martite. It comes in few colors such as metallic grey and dull to bright red oxygen ions in hematite take a hexagonal close-packed structure, with Fe^{+3} occupying octahedral sites.

2.1.2. Magnetite (Fe_3O_4)

It has many names but commonly black iron oxide. When it is obtained as a naturally magnetized magnetite, it is called loadstone. Some of its other names include Hercules stone, magnetic iron ore and ferrous ferrite. Magnetite as a transition metal oxide exhibits the strongest magnetism [23, 26]. Due to its relatively small bandgap of 0.1eV, it is known as the

iron oxide with the least resistivity and can also exist as both n- and p-type semiconductors [27]. The oxygen ions in magnetite are in a cubic close-packed structure. Magnetite has an inverse spinel structure with Fe^{+3} spread randomly between octahedral and tetrahedral sites and Fe^{+2} in octahedral sites.

Table 2. 1 Physical and magnetic properties of iron oxide [24]

Property	Hematite	Magnetite	Maghemite
Molecular formula	α- Fe_2O_3	Fe_3O_4	γ- Fe_2O_3
Density (g/cm^3)	5.26	5.18	4.87
Melting Point (℃)	1350	1583-1597	-
Type of magnetism	Weakly ferromagnetic or antiferromagnetic	Ferromagnetic	Ferrimagnetic
Curie temperature (K)	956	850	820- 986
Ms at 300 K $A-m^2/kg$)	0.3	92-100	60-80
Crystallographic system	Rhombohedral, hexagonal	Cubic	Cubic or tetrahedral
Structural type	Corundum	Inverse spinel	Defect spinel
Space group	R3c (hexagonal)	Fd3m	$P4_332$ (Cubic); $P4_14_14_1$(tetragonal)
Lattice parameter (nm)	α = 0.5034, c = 1.375 (hexagonal) $\alpha_{Rh} = 0.5427$, α=55.3° (rhombohedral)	α = 0.8396	α = 0.83474 (Cubic), α = 0.8347, c = 2.501 (hexagonal)

2.1.3. Maghemite (γ- Fe_2O_3).

It is found in soils as a broken down product of magnetite. This is considered as a fully oxidized magnetite due to its crystal constituents and an *n*-type semiconductor with a 2.0eV bandgap. In maghemite, just as in magnetite, the oxygen ions are arranged in a cubic close-packed structure. The spinel structure possessed by Maghemite, unlike magnetite, has vacancies in its cation sublattice. The Fe^{+3} are regularly arranged and occupy two-thirds of the sites, with one vacant site following two filled sites [23].

2.2. Type & Magnetic Behaviour of Iron Oxide

The magnetic moments in iron atoms are very strong, resulting from four unpaired electrons in its 3d orbitals. Paramagnetic, ferromagnetic, ferrimagnetic and antiferromagnetic are the various magnetic states attainable in the crystal forms of iron atoms. In its paramagnetic state (Figure 2(a)), atomic magnetic moments are randomly aligned with respect to each other yielding a zero magnetic moment. When exposed to an external magnetic field, there could be the alignment of some of these moments to result in a small net magnet moment. If the magnetic moment remains aligned after the removal of the external magnetic field, then a ferromagnetic (Figure 2(c)) state is reached. A ferrimagnetic state (Figure 2(b)) is reached when the crystal has a net magnetic moment from two types of atoms with moments of different strengths arranged in an antiparallel manner. If the magnetic moments are of the same magnitude which is not the case for the ferrimagnetic, then the crystal is antiferromagnetic (Figure 2(d)) and possesses no net magnetic moment.

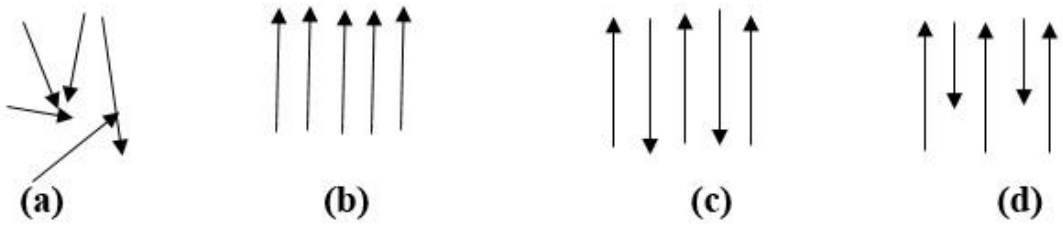

Figure 2. 2 Magnetic States (a) Paramagnetism (b) Ferromagnetism (c) Anti Ferromagnetism (d) Ferrimagnetism

2.3. Synthesis of Iron Oxide Nanoparticles (IONPs)

Nanomaterials are produced through different routes which include conventional and chemical synthesis approaches. Considering the conventional nanoparticle synthesis approach (e.g., attrition and pyrolysis, etc.), its drawbacks include defective surface formation, low production rate, high cost of manufacturing, and large energy requirement [28]. Chemical synthesis approach (e.g., chemical reduction, sol-gel technique, etc.) involves the usage of toxic chemicals, formation of hazardous by-products, and contamination from precursor chemicals [28].

Efficient synthesis approaches geared towards the production of stable, biocompatible shape controlled and monodispersed iron oxide nanoparticles have been described in reports from the much research developed to the synthesis of iron oxides NPs over the years. Currently, a variety of synthesis methods tested include co-precipitation, thermal decomposition, hydrothermal and solvothermal syntheses, sonochemical synthesis and biological synthesis. Some other methods also used in preparing these NPs are electrochemical synthesis [29, 30], laser pyrolysis techniques [31], and microorganism or bacterial synthesis (which include the Magnetotactic and iron reducing bacteria) [32, 33], etc.

Each synthesis approach entails many processes which affect the size, morphology, properties and composition of iron oxides produced. Also, they possess advantages and disadvantages affecting the iron oxides' applications.

2.3.1. Co-Precipitation

The co-precipitation approach is the most conventional synthesis method used in obtaining Fe_3O_4 or γ- Fe_2O_3. In this approach, Fe^{3+} and Fe^{2+} are mixed in a ratio 1:2 in a very basic solution at room temperature or at elevated temperatures. The basic solvent is required because, when the pH is less than 11, the nucleation of Fe_3O_4 is easier and with pH is higher than 11, growth is favoured. The method is simply represented with

$$Fe^{2+} + 2Fe^{3+} + 8OH - \leftrightarrows 2Fe(OH)3 \longrightarrow Fe_3O_4 \downarrow + 4H_2O$$ ---------- *Equation 1[24]*

The particle size control, composition and morphology in the co-precipitation pathway is restricted with reason that growth is kinetically controlled by the particle [24]. The size, shape and composition controlling factors of the iron Oxide NPs are the ferric and ferrous ions ratio, the type of salt used (chlorides, nitrates, sulphates etc.), the pH value, ionic strength of the medium, the reaction temperature and other parameters (example; stirring rate). For instance, the co-precipitation agent used by Blanco-Andujar et al in synthesizing IONPs was sodium carbonate, the reaction took place adequately slowly, enabling a thorough examination of both the pathway of the reaction and products formed [34].

The co-precipitation approach is successful and traditional methods employed for the synthesis of Fe_3O_4 nanoparticles having high saturation magnetization but with shortcomings such as the broad particle size distribution, and the use of a strong base in the reaction process. With the co-precipitation method, there is also a reduced success possibility of obtaining monodispersed NPs. The experiments lead to the production of wastewaters with basic pH values Wastewaters

having very basic pH values are produced in the experiment, which needs further treatments in other to protect the environment. Another disadvantage of these aqueous solutions synthesis is the need for adjusting of the pH values of the reaction mixture in both the synthesis and purification steps [24].

Currently, aggregation and biocompatibility problems of IONPs can be blamed for hindering the applications in biomedical fields.

2.3.2. Thermal Decomposition

In the above-described synthesis route, the rate at which the particles are formed is fast and therefore controlling the size of the formed particles and their distribution is hard. To curb such problems, various alternative approaches have been developed which include a non-aqueous approach like the thermal decomposition approach. This thermal decomposition method can be further divided into 2; the hot-injection approach and the conventional reaction approach. The Hot-injection approach involves the injection of the precursors into a hot reaction mixture whereas conventional reaction approach, involves the preparation at room temperature, a reaction mixture then heating it in a closed or open reaction vessel.

Most reactions carried out at room temperature, give rise to IONPs of low crystallinity which is observed in the co-precipitation approach. Thermal decomposition involving high temperature produces higher monodispersed, narrow size distribution and highly crystalline magnetic IONPs of coordinated iron precursors in organic solvents. This is due to the fact that, nucleation in the thermal decomposition approach involving high temperatures, can be separated from growth, which is not in the case of co-precipitation, and intricate hydrolysis reaction can be side-stepped [35, 36].

In the synthesis of iron oxide nanoparticles and decomposition of ferric salts such as Fe(Cup)3 (cup = N-nitrosophenylhydroxylamine) [37, 38], Fe(acac)3 (acac = acetylacetonate) [39], $Fe(CO)_5$ [40], iron oleate [41], Prussian blue ($Fe_4(Fe(CN)_6 \cdot 14H_2O$) [42, 43] , Fe– urea complex ($(Fe(CON2H4)_6)(NO_3)_3$) [44], ferrocene (Fe ($C_5H_5)_2$) [45] and $Fe_3(CO)_{12}$ [46], a phase decomposition path involving organic solution has been often employed, followed by oxidation. This can lead to monodispersed IONPs of high-quality, requiring relatively higher temperatures and a complicated operation. This complicated operation includes the involvement of a stabilizer that can reduce the rate of the nucleation and inhibit additives absorption onto the growing nanocrystals and nuclei resulting in the formation of small iron oxide nanoparticles (inhibits growth) [47]. Stabilizers used include oleic acid, 1- octadecene, 1-tetradecene, and oleylamine. The size distribution of IONPs products which are usually spherical can be controlled to some extent with particle sizes below 30nm. Even though the production of highly monodispersed particles with narrow size distribution is an advantage of the thermal decomposition method, it is highly disadvantaged by its resulting NPs being generally only dissolvable in nonpolar solvents.

2.3.3. Hydrothermal Synthesis and Solvothermal Synthesis

The strong correlation between parameters such as controlled shape and size and magnetic properties make IONPs possessing such parameters technologically vital. Whereas the thermal decomposition approaches usually lead to an intricate process or involve relatively high temperatures, an alternative, hydrothermal synthesis, comprises several wet chemical technologies of crystallizing substance in a closed container from the high temperature aqueous solution (ranging from 130 to 250℃) at high vapour pressure (ranging from 0.3 to 4 MPa) [47]. This method has been employed in growing single crystal particles which are dislocation-free, and grains formed from this approach could possess a better crystallinity as compared to other

approaches. The hydrothermal synthesis can therefore easily yield highly crystalline iron oxide nanoparticles which include γ- Fe_2O_3, Fe_3O_4 and α- Fe_2O_3 nanoparticles [24]. Synthesis of IONPs using hydrothermal method has been reported by many authors [48-51].

The creation of unstable crystalline phases at the melting point is a likely advantage of the hydrothermal approach compared with the other crystal growth approaches [24]. Also, this approach allows the growth of materials close to their melting points at great vapor pressure [52]. This is again a very appropriate approach for growing good-quality Iron oxide nanocrystals with controlled composition. It has been shown that the big idea behind hydrothermal approach has been extrapolated to non-aqueous systems and yielded the 'solvothermal process' which uses an organic solvent as the reaction medium instead of water [24].

Furthermore, the hydrothermal and solvothermal approaches are easy and common methods for producing hollow IONPs. In the normal use of this approach, sodium citrate, acetate and urea are mixed with Fe^{3+} as the iron resource, in ethylene glycol under stirring. The resulting homogeneous dispersion is sealed to heat for 8-24h at about 200°C in a stainless steel autoclave, lined with Teflon [53-56]. Controllable size and shape IONPs are prepared using developed hydrothermal and solvothermal synthesis approaches [57-60]. The hydrothermal and solvothermal approaches are beneficial in producing shape-controlled IONPs.

2.3.4. Sonochemical Method

This method has been widely used to produce novel materials with uncommon properties. The sonochemical approach makes use of the chemical effects of ultrasound arising from acoustic cavitation (the formation, growth, and implosive collapse of bubbles in liquid) [47]. In this, method, ultrasound of higher intensity is used in producing novel structures and providing a

rare path to known materials, without long reaction times, high pressures or high temperatures [61]. Creation and oscillation of cavities (bubbles) are caused by the alternating expansive and compressive acoustic waves under ultrasound irradiation. The cavities can accumulate ultrasonic energy as they oscillate while growing to a particular size (normally tens of mm). Cavity overgrowth and collapse can occur under perfect conditions, leading to the release of the concentrated stored up energy within the cavity in a short period (at cooling and heating rate of $>10^{10}Ks^{-1}$). The cavitational collapse is confined and brief having 1000 bar and 5000 K of pressure and temperature respectively [47, 62, 63]. Various forms of bare and functionalized IONPs are prepared using the sonochemical approach by sonicating an aqueous ferrous or ferric salt solution. This process is usually done in presence of air [64-68].

Biocompatible IONPs can be synthesized using the sonolysis approach. For instance, the sonochemical method was employed by Zhu et al in the synthesis of Fe_3O_4 nanoparticles with 30–40 nm sizes and these nanoparticles were evenly spread on reduced graphene oxide (RGO) sheets (Fe_3O_4/RGO). A biosensor for sensing H_2O_2 was fabricated using this Fe_3O_4/ RGO immobilized with hemoglobin. The biosensor established a quick response to H_2O_2.

Some advantages of the sonochemical method include homogeneity of mixing and reduced crystal growth, possibly leading to accelerated effect in rate and mechanism of chemical reaction. However, the sonochemical method is not useful in the production of Iron Oxide nanoparticles with controllable shapes [24].

Table 2. 2 Comparing of the synthetic approaches for synthesizing magnetic iron oxide nanoparticles [24]

Methods	Reaction temperature (℃)	Reaction and conditions	Reaction period	Size distribution	Shape control	Yield
Co-Precipitation	20-150	Very simple, ambient	Minutes	Relatively narrow	Not good	High
Thermal decomposition	100-350	Complicated, inert atmosphere	Hours-days	Very narrow	Very good	High
Hydro or solvothermal synthesis	150-220	Simple, High pressure	Hours-days	Very narrow	Very good	High
Sonochemical	20-50	very simple, ambient	Minutes	Narrow	Bad	Medium
Biosynthesis	Room Temperature	Complicated, ambient	Hours-days	Broad	Bad	Low

In reference to Table 2.2 above, the five above briefly described synthetic approaches, have numerous advantages and disadvantages for preparing iron oxide NPs. Thermal decomposition and hydrothermal synthetic methods seem the optimal method when size and morphology control is required. To produce water-soluble and biocompatible iron oxide NPs, co-precipitation approach was used but offers low control of the particle shape, broad distributions of sizes and aggregation of particles. Considering the rate of production, the alternative, sonochemical approach can also be employed to synthesize IONPs.

In addition, it is important that some biological synthesis routes have been reported for environment protection purposes. For example, recently Bharde et al.[32] reported that the bacterium Actinobacter sp. is capable of synthesizing maghemite under aerobic conditions

when reacting with the ferric chloride precursors. Moreover, maghemite NPs showed superparamagnetic characteristics as expected. Also, Yew et al. used a green synthesis approach where a plant extract (Kappaphycus alvarezii (K. alvarezii)) was used as a mediator. An environmentally friendly Magnetic Fe_3O_4 was the resultant [69]. Below in Table 2.3, some green synthesized Fe_3O_4 nanoparticles are tabulated with their corresponding crystallite size and plants used in the synthesis.

Table 2. 3 Some Green synthesized Fe_3O_4, plants used and their crystallite sizes.

Plant Extract	Crystallite size	Reference
Green tea leaves	40-60 nm	[70]
Moringa oleifera Leaf	7 nm	[71]
Lagenaria Siceraria	30-100 nm	[72]
Seaweed	14.7 nm	[69]
Maize Silky Hairs	84.8 nm	[19]
Chinese cabbage	48.9 nm	[19]
Seaweed (Sargassum muticum)	17-25 nm	[73]
Musa ornata flower sheath	43.69 nm	[74]
Brown seaweed	10- 27.4 nm	[75]
Plantain Peels	Below 50 nm	[76]

2.3.5. Biological Synthesis (Biosynthesis)

The biological synthesis of nanoparticles is a rapidly growing field of research owing to their eco- friendly, cost-effective, simple and rapid production of nanoparticles. Some of the advantages of biological synthesis approach over the physical and chemical methods are;

a. clean and eco-friendly approach, since toxic chemicals are not employed [77].

b. reduced cost as capping and reduction is done by enzymes and phytochemical present in mediators[77].
c. large-scale production of small nanoparticles is possible [78].
d. Energy saving, as conditions like high energy and high pressure, are not required [79].

A widespread of biological resources like microorganisms and plants can be employed in nanoparticle synthesis [21]. Plant extracts are capable of reducing metal ions quicker compared to microbes. Depending on the plant type and phytochemicals present in the plants, the nanoparticles are synthesized in few minutes or hours, whereas microorganism-mediated methods require a longer time [22]. These reasons and the easy availability of plants in nature, make plants favorable biological resources than microbes. Therefore, for the sake of environmental protection, green chemistry and biological methods which include bacterially and plant induced synthesis of iron oxide NPs are important advances [47].

Metal and metal oxides nanoparticles produced through this approach can be engineered to be monodispersed by the regulation of synthetic parameter such as temperature, incubation period, mixing ratio and pH. The specific mechanism and components from the plant in this nanoparticles synthesis process are unclear. Some metabolites such as proteins, organic acids, vitamins, flavonoids, alkaloids, terpenoids, polysaccharides and polyphenols have been proposed to play a significant role in reducing of metal salts while stabilizing and capping nanoparticles during the synthesis [80]. For instance, the biomolecules in *Murranya Koenigii* leaf extract, have been reported to have facilitated the synthesizing and stabilizing of gold and silver nanoparticles. Also, *Corallina Officinalis* extract aided in synthesizing and stabilizing of gold nanoparticles and this was credited to the hydroxyl functional groups and carbonyl groups in the extract [81].

pH changes during plant-mediated synthesis of nanoparticles are capable of inducing changes in natural phytochemicals within plants and this may affect their binding and the reduction of

metal irons capabilities [13]. For instance, at high pH, tuber powder of Curcuma longa is suspected to contain many negatively charged functional groups, capable of binding effectively and reducing silver ions resulting in more nanoparticles being produced, in the synthesizing silver nanoparticles [82]. It has been proven also that in the synthesis of gold nanoparticle with pear fruit extract, alkaline pH yields hexagonal and triangular nanoparticles whereas acidic pH yields, not nanoparticles.

2.3.5.1. Advantages of green synthesis

In this synthesis approach, there is no need for further stabilizing agent owing to the fact that, the plant's constituents act as stabilizing and capping agents [83]. These synthesized nanoparticles adsorb biomolecules gradually and selectively unto their surfaces when in their complex biological fluids [13].

This leaves the particles with additional capabilities in their fields of application. This makes biologically synthesized nanoparticles more effective due to the adsorption of bioactive constituents onto their surface from the biological source eg. plant. In the use of medicinal plants in the synthesis of the nanoparticles, there exist many metabolites involved in pharmacological activity that are assumed to adsorb to the surface of the synthesized particles, providing extra benefits, as they enhance the efficacy of the nanoparticles [83-85].

The use of this synthesis route reduced the number of steps required in the attaching of functional groups to onto the surface of the nanoparticle to make them bioactive [86].

There is a need to select a plant with functional groups specific for the exact synthesis to be performed.

2.3.5.2. Maize Leaves Extract in Biosynthesis

Cereals serve as the main source of carbohydrates, proteins, vitamins and minerals [87]. Cereals contain biomolecules which are proteins and their derivatives, peptides and amino acids which exist in different quantities, which specific biological effects are able to promote health [88]. Maize, therefore, is one of the cereals that possess some bioactive peptides consisting of characteristic amino acid sequences which when exposing to the human system, display diverse functionalities. The maize plant contains four groups of storage proteins; albumins, globulins, prolamins and glutelins. This grouping is based on solubility; albumins are water soluble, globulins are soluble in salt solution, prolamins are soluble in alcohols and glutelins are insoluble in neutral aqueous solutions and ethanol. Generally, peptides derived from cereals have been shown to show antithrombotic, antihypertensive, anticancer [89] [90], antimicrobial and antioxidant properties [91].

Natural products derived from plants are very important in the field of chemotherapy [89]. Studies have reported that bioactive peptides are capable of inducing apoptosis in tumors. Bioactive peptides exhibit antitumor activity in a way that includes the induction of apoptosis [92], obstruction of a tumor intermediate production [93] and regulation of immune among others. As corn kernels stores all their proteins that are ever essential is cancer treatment, it evident that its leave will hold some of these.

2.3.5.3. Plantain Leaves and Peels Extract in Biosynthesis

Phytomedicine which is obtained from herbs in plants are widely used around the world and this is as a result of the numerous bioactive compounds contained in them. One of the plants with parts highly exalted around the world is the plantain. Its leaves play medicinal roles as well as the fruit which is believed to contain very required nutrients for dieting reasons. Plantain

contains many phenolic compounds and displays many biological functions mainly linked to their involvement in the stages of cancer [94]. Phytochemicals contained in plants extracts such as leaves, roots, stem and other parts are considered as metabolites to cure various kinds of diseases [95]. These bioactive groups play roles as antioxidants, preventing the release or production of free radicals which are associated with cancer, ageing, diabetes cardiovascular disorders etc. It has been reported that the phenol content of plantain at all stages of maturity is high and this makes it a right candidate being applied as a mediator for the synthesizing bio application related nanoparticles, hence cancer.

2.3.6. Biomedical Application

In these biomedical applications, two very important factors are biocompatibility and toxicity of IONPS. The parameter that determines the biocompatibility or toxicity is the size of the composite particle (core and coating) and the nature of the magnetic response. It is of high priority that the composite iron oxide nanoparticles have high magnetization so as to allow their motion in blood when under the control of external magnetic fields until reaching targeted pathologic tissue [96]. Traits of magnetic IONPs for medical application in vitro and in vivo are biodegradability, low toxicity and long blood retention time.

2.3.6.1. Cancer

Cancer refers to the abnormal growth of cells that undergo uncontrollable cell division and affect other cells at various parts of the body [97]. When changes in cell genes affect the normal growth of a cell or group of cells, the cells begin to multiply in an uncontrolled manner. These changes affect the normal functioning of cells such as their abilities to undergo repair, regeneration and apoptosis in times of cell damage. When damaged and unhealthy cells

undergo cell division rather than cell destruction, they become cancerous and spread uncontrollably to various parts of the body [97].

All parts of the body such as the lungs, breast, blood circulation etc., can be affected by cancer. Cancer is categorized in accordance with the type of tissue within which they occur. Cancers can be termed as carcinomas, sarcomas, myelomas or lymphomas when they appear in the epithelial tissues, connective tissues, plasma cells in the bone marrows and immune system cells respectively. Cancers which arise from two or more different tissues are termed as mixed cancers. Cancers are aggressive and life-threatening and can affect almost all the organs of the body. It is noted as one of the principal cause of death globally. The various forms of regular cancers include breast cancer, prostate cancer, lung cancer, colorectal cancer, liver cancer, ovarian and pancreatic cancer [98].

There are over 100 types of cancer and each poses different signs and symptoms depending on their size and location of cancer as well as the absence and presence of metastasis. Some common signs and symptoms of cancer include fever, pain, fatigue, unintended weight loss, skin changes, short of breath, changes or difficulty swallowing, lumps or tumors and many others. There are quite a number of treatment approaches but depend on the type and stage of cancer and most importantly the health of the patient. Some of these treatment procedures are radiation, surgery, angiogenesis inhibitors, cryosurgery and chemotherapy [99, 100]. Every treatment has its own potential risks, side effects and benefits. The seek for control over risks and side effects have set researchers on a path of finding other treatment process besides those already known.

2.3.6.2. Cancer Diagnostics and Treatment

Cancer is characterized by either failure of cellular apoptosis or uncontrollable cell growth. Apoptosis is the most important target in the treatment of various tumors [101]. Most chemotherapeutic drugs are geared towards inducing apoptosis in order to impede or stop the growth of cancer cells. These processes are facilitated by the presence of proteasomes in cells. The manipulation of proteasomal activities could normalize cellular homeostasis in cancer patients. With this as one way of treating cancer, it has set the stage for scientific research of proteasome inhibitors as a way to change this equilibrium in favor of apoptosis while reducing cytotoxicity of normal cells [102]. Recent studies have revealed that proteasome inhibitors effectively induce apoptosis in many types of cancer cells [103].

Clinical trials on a variety of diseases conducted, since late 1990, have led to the approval of proteasomes inhibitors to treat MM and mantle –cell lymphoma. Proteasome inhibitors have been tried severally on myeloma patients and found to produce initially great response but a resistance props up finally against these inhibitors. Investigating the cause and mechanism of this resistance is important to research on proteasomes inhibitors.

2.3.6.3. Apoptosis and Cancer

Apoptosis is used to describe cell death, which is vital in both controlling damaged cell removal and cell numbers all through development. Imperfect or faulty apoptosis is the breeding ground for numerous diseases including some cancers such as Leukaemia(B-CLL), where quiescent Tumour cells accumulate [103]. Apoptosis is initiated either by reason of cell stress or signals from other cells. It's the process behind the separation of toes in an embryo for example. As cancer is related to uncontrollable growth and spreading of abnormal cells, when signaled, apoptosis can be responsible for killing these abnormal cancer cells [104]. Cancer cells have

an abnormal apoptotic signaling pathway and this suppresses apoptosis [104]. This abnormal control of internal cell suicide provides many advantages to cancer cells aiding their resistance to chemotherapy. Interestingly, the most important factors associated with the control of apoptosis are controlled by some kind of proteasome (26S proteasome complex) [105, 106]. Cancer cells will be killed when apoptosis is promoted by way of inhibiting the proteolytic function in the cells. Inhibiting the proteolytic functions of the 26S proteasome make them aid apoptosis in some cancer cells [106].

Fe_3O_4 magnetic nanoparticles can be considered a strong candidate for cancer treatment owing to its strong proteasome inhibitory ability. Jayanta et al. reported Fe_3O_4 magnetic nanoparticle at a concentration of 100 and 10ug/ml showed proteasomal activity inhibition of 78.11% and 51.73% respectively [12]. In their research, the proteasome potential of Fe_3O_4 nanoparticles examined using a 20S proteasome assay kit for drug discovery (ENZO Life Sciences, Farmingdale, NY) in accordance with the manufacturer's procedures. Expoximcin at 0.56 and S.56 ug/ml and Fe_3O_4 at 10 and 100ug/ml as standard reference compounds were applied for the assay. In their work, the proteasomal inhibitory activity of Fe_3O_4 was investigated based on fluorescence intensity at an excitation and emission of 350 nm and 440 nm respectively, all at a reaction temperature of 30℃ using microplate readers.

As human cancer cells exhibit high levels of proteasomal activities, inhibiting them will be a new approach to treating cancer [107]. Proteasome inhibitors such as Fe_3O_4 are currently used in conjunction with anti-cancer drugs, due to the reported cancer cell resistance to these anti-cancer drugs [107].

Reactive oxygen species (ROS) are radical or molecules have single unpaired electrons in the outer shells. They are secondary messengers in cell signaling and vital for processes in normal cells. A redox imbalance may signal the presence of diseases which include cancer. On the

other hand, ROS production is a pathway selected by chemotherapy, radiotherapy and other cancer treatment approaches since they can aid in triggering internal cell death (apoptosis). Owing to the double roles played in ROS in the determination of cell fate, antioxidants therapies have been listed as a cancer treatment mechanism. Much research is ongoing in this field due to this nature of ROS [108].

2.3.6.4. Cell Signalling and Cancer

Cells are generally grouped into two, thus excitable and non- excitable cells. Many cells try to maintain an equilibrium potential. The group of cells that return to their equilibrium potential after the removal of a current applied for a short period are called non- excitable cells [109]. An example is the epithelial cells that line the gut walls. Cardiac cells, secretory cells and most neurons are members of the excitable cells which upon the application of a current strong enough, an action potential is generated before eventually returning to equilibrium [109].

Cell activities are governed and coordinated by a communication processes known as cell signalling. The ability of cells to respond appropriately to changes within their immediate surroundings contributes to the development of cells, repair of tissues and immunity. Disease such as diabetes, cancer and autoimmunity are associated with faulty signalling or signal processing [110].

One of the major tools of cell signalling is ion channels. Studies has established the fact that these ion channels contribute greatly to the basic cellular behaviour such as, the maintenance of tissue homeostasis in cell processes like proliferation, differentiation and apoptosis [111-116]. In physiological and pathological conditions, maintenance of tissue homeostasis requires the exchange of electrical charges across the surface of the cell membrane. The alteration of the charge distribution to allow the selective diffusion of certain ions such as K+, Ca++, Na+ and Cl- across the surface membranes results from the opening of ion channels[117] . Ion channel mechanisms include cell volume regulation, provision of influx of important signalling

ions, maintaining the membrane potential and controlling the volume of cells, which all occur in the life cycle of the cell [116, 118].

The voltage across cell membrane is the membrane potential (Vm) and result from the existence of these different ion channels with particular ion permeability [119]. The membrane potential in cancer cells can portray 2 major conditions, a hyperpolarization and depolarization. The resting membrane potential of a neuron is -60 to -70 millivolts, meaning that the cell at rest is more negative than its extracellular environment [120]. This charge difference between the cell and its surroundings can be altered depending on the flow certain ions such as Cl- into or K+ out of the cell [120]. When the membrane potential at specific parts of the neuron acquires a more negative charge relative to other parts of the neuron, the neuron is termed as hyperpolarized. However, when ions such as Na+ found in the extracellular surroundings of the neuron flows through ion channels into the cell, the membrane potential of the neuron increases and thus becomes more positive. This change resulting in a less negative charge of the membrane potential is termed as depolarization [120].

Cell proliferation at a point will yield “swelling”, a strictly controlled process that involves the activities of K+ and Cl- channels, when depolarized. These same ion channel mechanisms responsible for cell proliferation are also responsible for apoptosis, when hyperpolarized [118]. Cell shrinkage is characteristic of apoptosis, but the mechanism and role of this process in cell death are poorly understood [121-123]. Apoptosis is enhanced where the intracellular K+ (a cation) concentration is reduced and inhibited when K+ (a cation) influx occurs. Research has shown that the efflux of cations potassium K+, plays an important role in the cell death program [121]. In contrast, the extracellular environment at the same time contains low concentration of potassium and high concentration of sodium. The passive movement of potassium from the cell is enhanced by the net electrochemical gradient created irrespective of the negativity of the

transmembrane potential. The reduction in cell volume during cell death can therefore be contributed to the selective movement of ions such as potassium from the cell [121].

CHAPTER THREE

3.0. MATERIALS AND METHODS

3.1. Chemicals

All the reagents used in this work were of analytic grade and were used as received without additional purification. In the experimental process, Ferrous Chloride (tetrahydrate)[iron(II) chloride] $FeCl_2$. $4H_2O$ M.W. 198.81, ferric chloride [Iron(III) chloride] hexahydrate $FeCl_3$. $6H_2O$ M.W. 270.296 and Sodium hydroxide were the chemical used. $FeCl_2$. $4H_2O$ was purchased from Research-labs, $FeCl_3$. $6H_2O$ from Daejung chemicals and NaOH for Sigma-Aldrich.

3.2. Collection of Plant Materials

Two plants were used; Maize and plantain. The extracts were prepared from plantain leaves, plantain peel and maize leaves. The plantain leaves were collected from a small plantain farm on University of Ghana campus (Legon campus, Ayido flat E). The plantain peels were collected from plantain fruits purchased from Tesano Market. The Maize blade leaves were collected from maize plants on a small maize farm in Ashalaja.

3.3. Preparation of Aqueous Extract

In preparing the extracts, each plant part (maize leaves, plantain peels and plantain leave) was rinsed three times using distilled water, for the removal of dust. They were cut into smaller sizes and dried in a GeblabPrime oven at 60 °C for 3 days after which they were then ground/milled into powder using the Ika A11B mill. The grinding was done for approximately 10 minutes. 20 g of the powder was measured into a 300 mL beaker and 200 mL of distilled

water added. The mixture was heated at 70 ℃ for 1 hour, on a hot plate, with continuous stirring. The mixture was then filtered, first with a cheesecloth and then with filter paper. The extract obtained was then stored at -4 ℃ before being used for the synthesis of the Fe_3O_4 magnetic nanoparticles. Images of the process are displayed in Figure 3. 1 below. The process is summarized in the flowchart in Figure 3. 2 below.

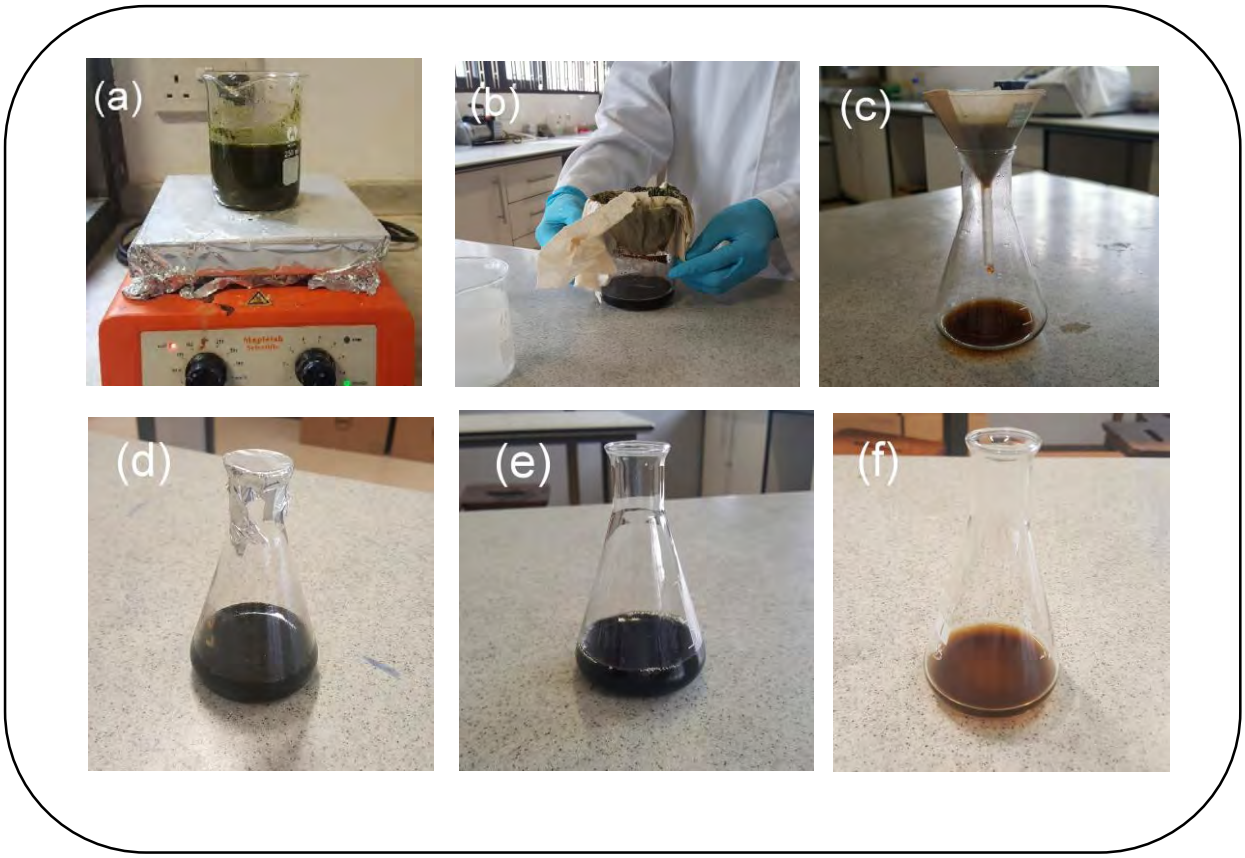

Figure 3. 1 The plant extract preparation (a) Heating of Powder in Water (b) Filtering with a cheese cloth (c) Filtrating with filter paper (d) Plantain Leaves Extract obtained after Filter paper filtration. filtration (e) Maize leaves Extract obtained after Filter

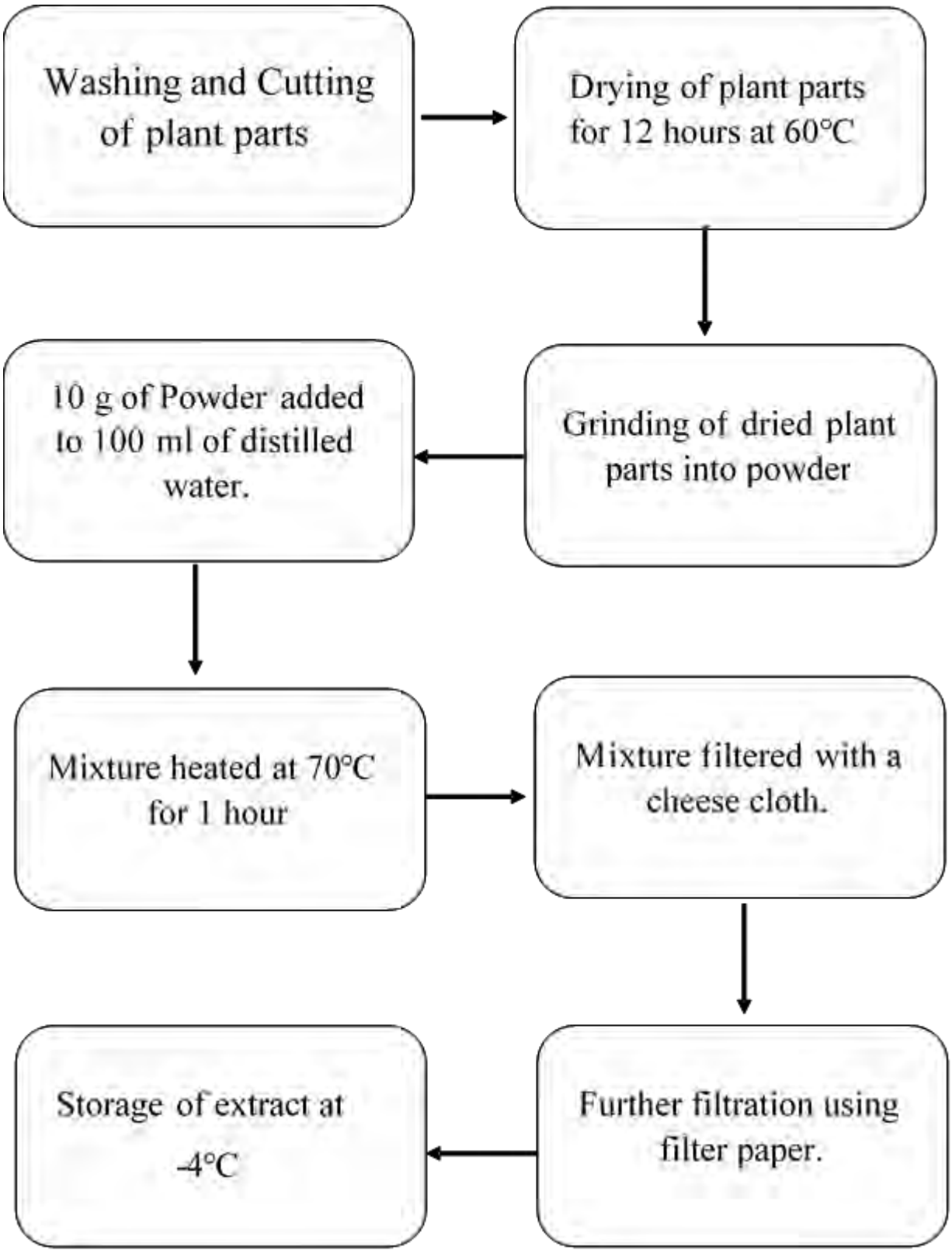

Figure 3. 2 Flow chat of plant extract preparation

3.4. Synthesis of Magnetic Fe_3O_4 Nanoparticles

In synthesizing of the Fe_3O_4 magnetic nanoparticles, $FeCl_3$ Hexa-hydrate and $FeCl_2$ tetra-hydrate were the precursors used and plantain leaves or maize leaves or plantain peels extract as reducing and stabilizing agents separately. Prior to the commencement of the synthesis, 2.0 M of NaOH was prepared by dissolving 16 g of NaOH pellets in 200 mL of distilled water. Different molar ratios of $FeCl_3$ Hexa-hydrate and $FeCl_2$ tetra-hydrate precursors were used, 2:1 2:2 molar ratios and 2:1 (greater masses).

In the 2:1 molar ratios, 5.52 g and 10.82 g of $FeCl_3$ Hexa-hydrate were mixed with 1.98g and 3.97 g of $FeCl_2$ tetra-hydrate respectively. In the 2:2 molar ratios, 10.82 g of $FeCl_3$ Hexa-hydrate was mixed with 7.97 g of $FeCl_2$ tetra-hydrate were used.

The mixture of the precursors was dissolved in 200 ml of distilled water and stirred for 20 minutes under continuous laboratory light source. 40 ml of the extract was then added to the precursor solution changing the color of the solution from pale yellow to dark green (plantain leaves and peels extract) and light black (Maize leaves extract). NaOH was added 3 mL/min to permit uniform formation of the magnetic Fe_3O_4 nanoparticles in the reaction mixture (till pH of 11 was attained). The color changed from the precursor and extract solution colors to brown when pH between 3-4 was recorded and to black when pH of 8-11 was recorded. After the completion of the reaction, the black colored nanoparticles such as PPeels Fe_3O_4NPs (PP-FePs), PLeaves Fe_3O_4NPs (PL-FePs) and MLeaves Fe_3O_4NPs (ML-FePs) settled at the bottom of the solution and with the aid of an external magnet, distilled water was used to wash the particles 3 times. The washed particles were then dried in an oven at 50 ℃ till they were very dry for 8 hours. Some of the particles were freeze-dried. The dried samples bottled and stored at room temperature. In Figure 3.3 below, the color changes observed during the synthesis and the separation of the particles for washing are shown. Figure 3.4 below shows a summary of

the entire synthesis process. In Table 3.1, the different molar ratios of precursors used in the synthesis and their corresponding nanoparticle sample names are tabulated.

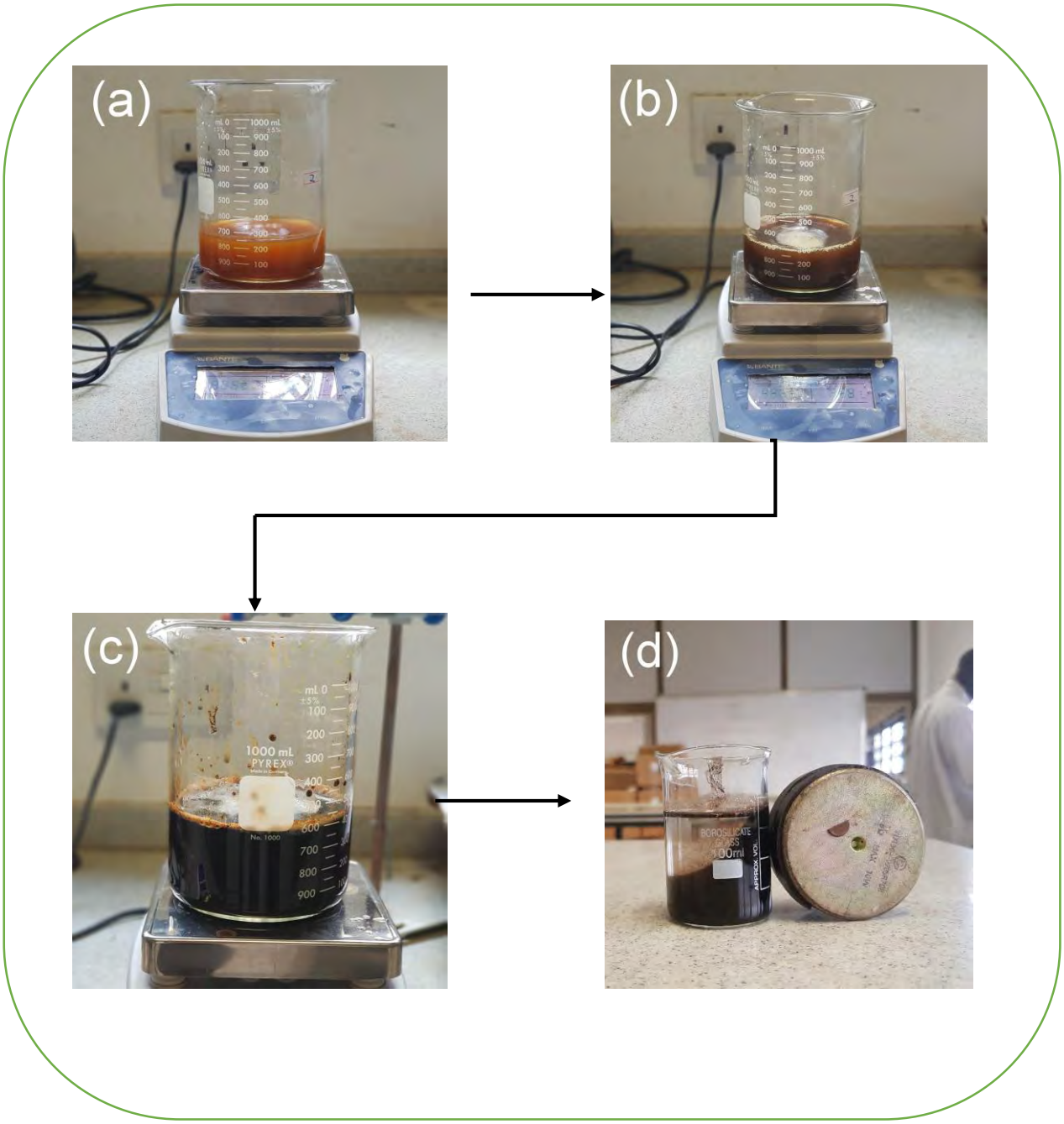

Figure 3. 3 Colour changes separation of particles in Synthesis of Fe_3O_4 NPs (a) Fe^{3+} and Fe^{2+} (b) Fe^{3+} and Fe^{2+} and Extracts (c) Fe^{3+} and Fe^{2+} and Extract and NaOH (d) Separation of Synthesised particles with external magnet.

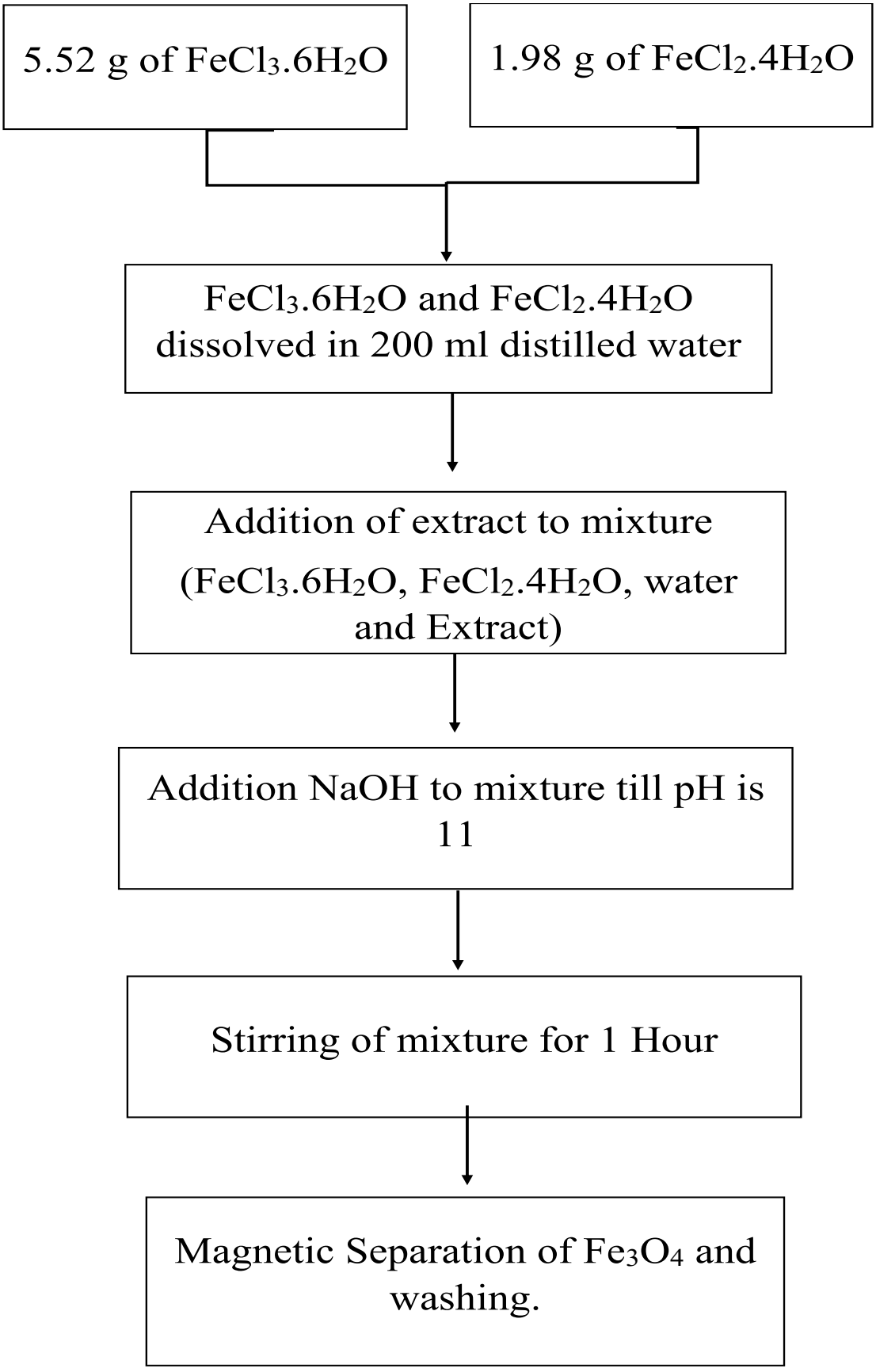

Figure 3. 4 Flowchart for Synthesis of Fe_3O_4 NPs (using the 2:1 ratio)

Table 3. 1 Samples names and their corresponding preparation molar ratios of precursors.

Extract used	**Fe^{3+} Mass used**	**Fe^{2+} Mass used**	**Molar Ratio**	**Sample Name**
Maize Leaves	5.52	1.98	2:1	ML1-FePs
	10.82	3.97	2:1	ML2-FePs
	10.82	7.97	2:2	ML3-FePs
Plantain Leaves	5.52	1.98	2:1	PL1-FePs
	10.82	7.97	2:2	PL3-FePs
Plantain Peels	5.52	1.98	2:1	PP1-FePs
	10.82	3.98	2:1	PP2-FePs
	10.82	7.97	2:2	PP3-FePs

3.5. Characterisation of Fe_3O_4.

After the synthesis, ML-FePs, PL-Fe NPs and PP-FePs were characterized to identify their physical and chemical properties by Scanning electron microscopy (SEM), UV-Vis Spectroscopy, X-ray diffraction (XRD), Cyclic voltammetry (CV), Energy- Dispersive X-Ray Spectroscopy(EDX) and Fourier-transform infrared spectroscopy (FT-IR).

A first step for identifying the Fe_3O_4 NPs formation was the change in color of the precursor solution with visual inspection. The change of the color of the mixture to a deep black mass of particles was used to identify, by observation, the forming of the Fe_3O_4 in solution.

3.5.1. UV-Vis Spectroscopy.

The UV-Visible spectroscopy (UV-Vis) is the absorbance spectroscopy with the UV- Visible regions. The process makes use of light within the visible and near-UV and near- infrared regions.

The synthesized particles were maintained in solution during this characterization process. For each of the samples, a time-dependent absorbance was investigated. From the commencement of stirring, after the pH of the solution reached 11, to an hour, at 10 minutes' interval, the UV-Vis Spectra was taken for the samples. The wavelength range used was 300-800 nm. The UV-Vis characterisation was done to check for the formation of the Fe_3O_4 in the process, thus comparing the spectra to that in literature.

3.5.2. X-Ray Diffraction Analysis (XRD)

After each synthesis, each sample obtained was placed in a plastic container and sealed. These washed magnetic samples where then taken for X-ray Diffraction analysis. Here, the analysis was conducted using Copper as the Anode material, K-Alpha1 [Å].

3.5.3. Scanning Electron Microscope (SEM)

The synthesized particles samples were freeze-dried for before the scanning was done using a Phenom desktop SEM.

3.5.4. Energy –Dispersive X-Ray Spectroscopy (EDX)

The EDX was conducted to obtain the elemental constituents on the synthesized particles to verify the formation of Fe_3O_4 nanoparticles. The Phenom desktop SEM also produced the EDX data.

3.5.5. Fourier- Transform Infrared Spectroscopy (FTIR)

FTIR was employed to help identify the functional groups of active compounds within a sample, by considering band and peak valve in the infrared radiations region. FT-IR spectroscopy characterization of the synthesized particles was conducted to identify the groups responsible for reducing and stabilization of the prepared particles [124] and also to look out for the formation of the Fe_3O_4. The Fourier-transform Infrared spectroscopy analysis conducted was done using PerkinElmer Spectrum Two, making use of the particulate form of the samples in the analysis. The particles were compacted unto the small sample holding diamond slit. The analysis was then conducted after a hammer was used to compress the sample in place.

3.5.6. Cyclic Voltammetry (CV)

The Cyclic Voltammetry is employed to study the electrochemical performance of the working electrode. This analysis was to inspect the redox nature of the Fe_3O_4 particles. The CV analysis was inspecting the flow of ions between the Fe^{3+} and Fe^{2+}, when in solution, which is characteristic of the Fe_3O_4 nanoparticles. Also, it was used in inspecting the change in current flow as the cancer cells were mixed with the Fe_3O_4 nanoparticles. The sample particles were mixed with water and placed on a contact electrode prob.

3.6. Testing of Fe_3O_4 Nanoparticles on Hela Cells (Cancer Cells)

In the testing of the Fe_3O_4 –NPs, culture Hela Cells were used. 2.0 mg of each sample of synthesized Fe_3O_4 –NPs, was mixed with 40 μL and Vortex for 3 minutes yielding a concentration of 50 mg/mL . To 100 μL of Hela Cells 5 μL of each synthesised Fe_3O_4 –NPs sample was added and the CV analysis conducted. 5 μL of Fe_3O_4 NPs was added to each mixture after 30 minutes and the CV analysis conducted until a total of 20 μL of Fe_3O_4 NPs

had been added (thus after 1 hours and 30 minutes to total 2 hours). Below in Figure 3. 5 is the flow chart summarizing the entire testing process. While doing this, a blank was run on the side with the addition of equal volumes of distilled water to the Hela cells instead of Fe_3O_4 NPs at same time interval.

Often in cancer treatment using Fe_3O_4 –NPs, they are used in conjunction with chemotherapy drugs. In this testing, Fe_3O_4 NPs are used alone.

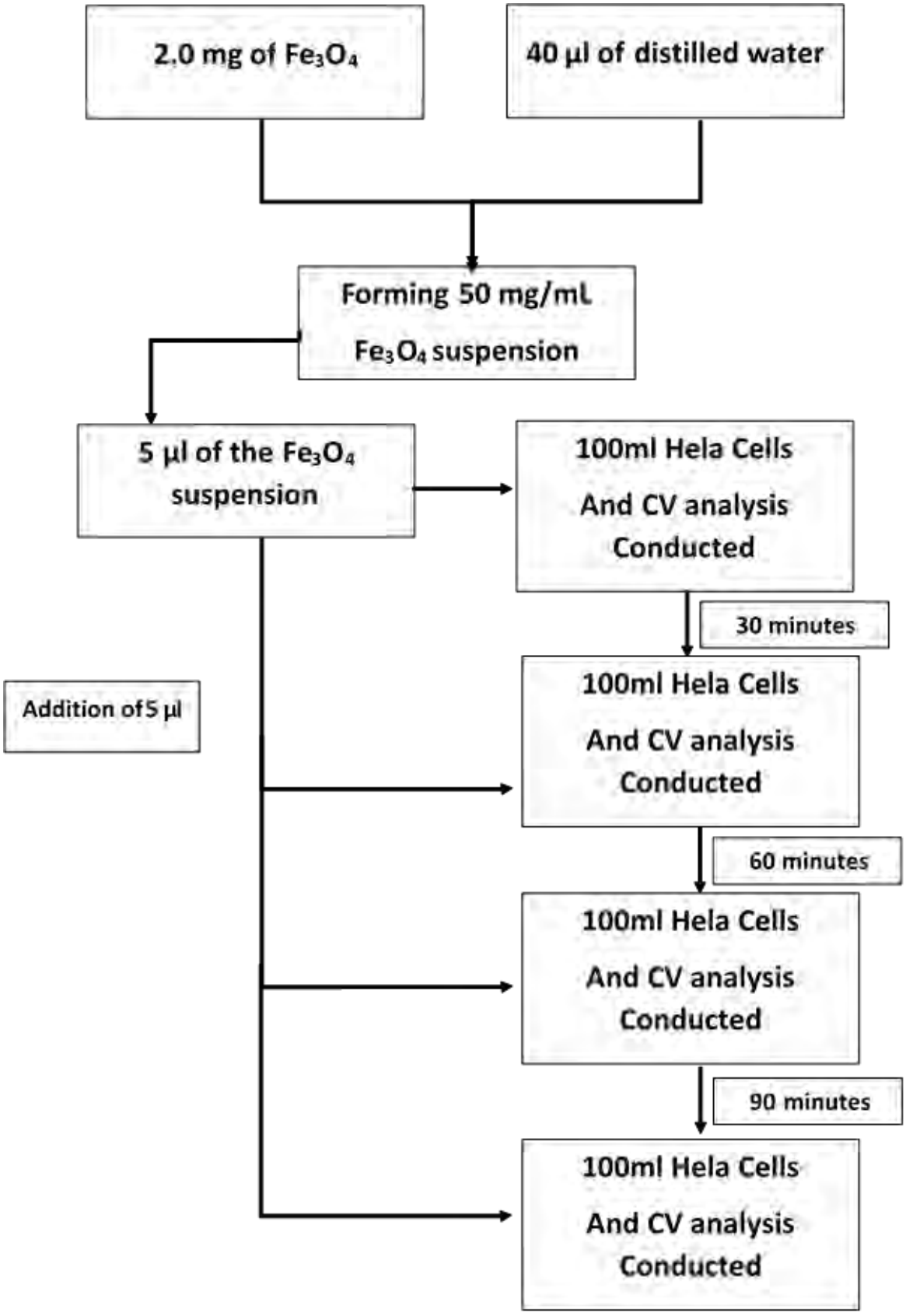

Figure 3. 5 Flowchart for NPs Testing on Hela Cells

CHAPTER FOUR

4.0. RESULTS AND DISCUSSION

In this chapter, results obtained from the characterization of the synthesized particle and their effect on the application on Hela Cells (Cancer Cells) will be displayed and discussed. After the Scanning Electron Microscope (SEM), UV-Vis Spectroscopy, X-ray diffraction (XRD), Cyclic voltammetry (CV) and Fourier-transform infrared spectroscopy (FT-IR) characterizations, below are displayed the results.

4.1. UV-Vis Spectroscopy

The synthesized Fe-NPs were preliminarily confirmed by the UV-Vis spectra recording at a range of 300-800 nm after the pH of 11 was attained during the synthesis.

When a pH of 11 was reached, after the addition of NaOH, the UV-Vis spectra at 10 minutes' intervals to an hour was taken. For all the synthesis conducted with the various extracts, a similar pattern was recorded. The UV-Vis Spectra for the 1 hour stirring time is shown in Figure 4.1 below.

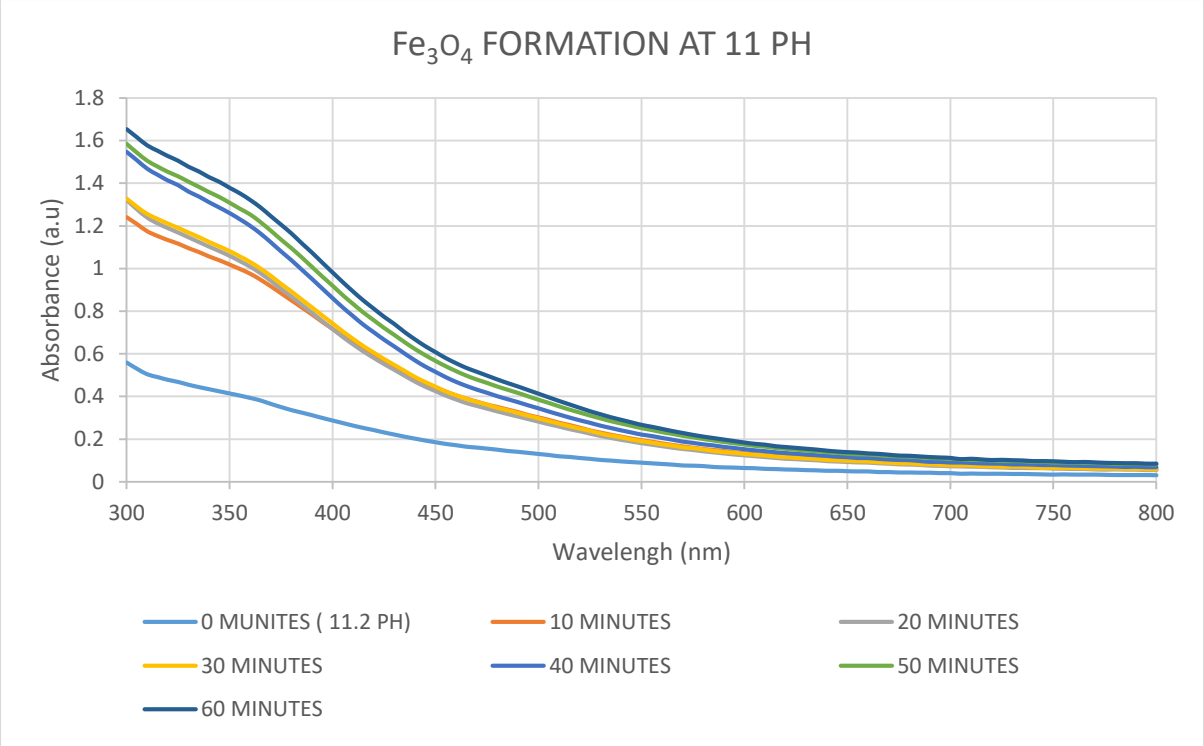

Figure 4. 1 UV Vis Spectra of particle formation at 10 minutes' interval

The UV Vis spectra show a progressive increase in particle concentration, hence absorbance, as stirring time increases. The absorbance range (300 -600 nm) of the UV-Vis Spectra obtained tallied with the pre-existing magnetic Fe_3O_4 NPs spectra, showing continues absorbance in the visible range [125-127]. The UV-Vis spectra for the Fe_3O_4 NPs synthesised was similar to that of Yew et al. reported using seaweed (Kappaphycus alvarezii) extract [69] and that reported by Basavegowda et al. using P. frutescens extracts [125] .

In the formation of Fe_3O_4 NPs, two major pH points were resting points. These resting points were around 3-4 pH and 8-9 pH. These stop points are important for the formation of the nanoparticles, thus, at around 3-4 pH, the precipitation of Fe^{3+} occurs and that of Fe^{2+} occurs at around 8-9 pH [128]. After these precipitations of Fe ions occur, the formation of the Fe_3O_4 NPs particles take place by the combination of these ion in the lattices which require time. Approaching the 60-minute time, the absorption remained almost the same which is suspected

to be as a result of nearness to the completion of the formation of the particles. The pattern of the spectra agrees with literature in that, there is a steady increase in absorbance, starting from around 650 nm [129]. The steady increase within the 650nm to 400nm indicates that the synthesised Fe_3O_4 NPs absorbs light in the visible range and the continues rise between 400nm to 300nm also indicates a slight absorbance in the UV range.

The UV-Vis confirms this by the increasing absorbance as stirring time increases, to show that particle formation increase with the increasing time.

The UV-Vis Spectra, when compared with literature, confirmed the Fe_3O_4 NPs formation [69, 125-127]. The Spectra and the attraction of the particles in solution pointed to the particles being magnetic Fe_3O_4 NPs.

4.2. Fourier- Transform Infrared Spectroscopy (FTIR)

FT-IR spectroscopy conducted was to identify the functional groups present in maize leaves, plantain leaves and plantain peels which aided in synthesizing the Fe_3O_4–NPs, acting as stabilizers and reducers. The FTIR spectra of synthesized NPs obtained were within 3500–450 cm^{-1}.

The spectra of the all extract shown in Figure 4. 2, revealed strong absorption bands at ~3348, ~2921, ~2845, ~1637 and ~1036. The region of ~3348 cm^{-1} displayed bands corresponding to –OH (of phenol compound) stretching vibrations. The absorption peaks at ~2921 cm^{-1} and 2845 cm^{-1} are associated with the sp3 C–H stretching vibrations of the $–CH_2$ functional group [130]. The peak at ~1637 cm^{-1} represents N-H bending of amide group and the peak at ~1036 cm^{-1} correspond to C-N stretching of aliphatic amines [131].

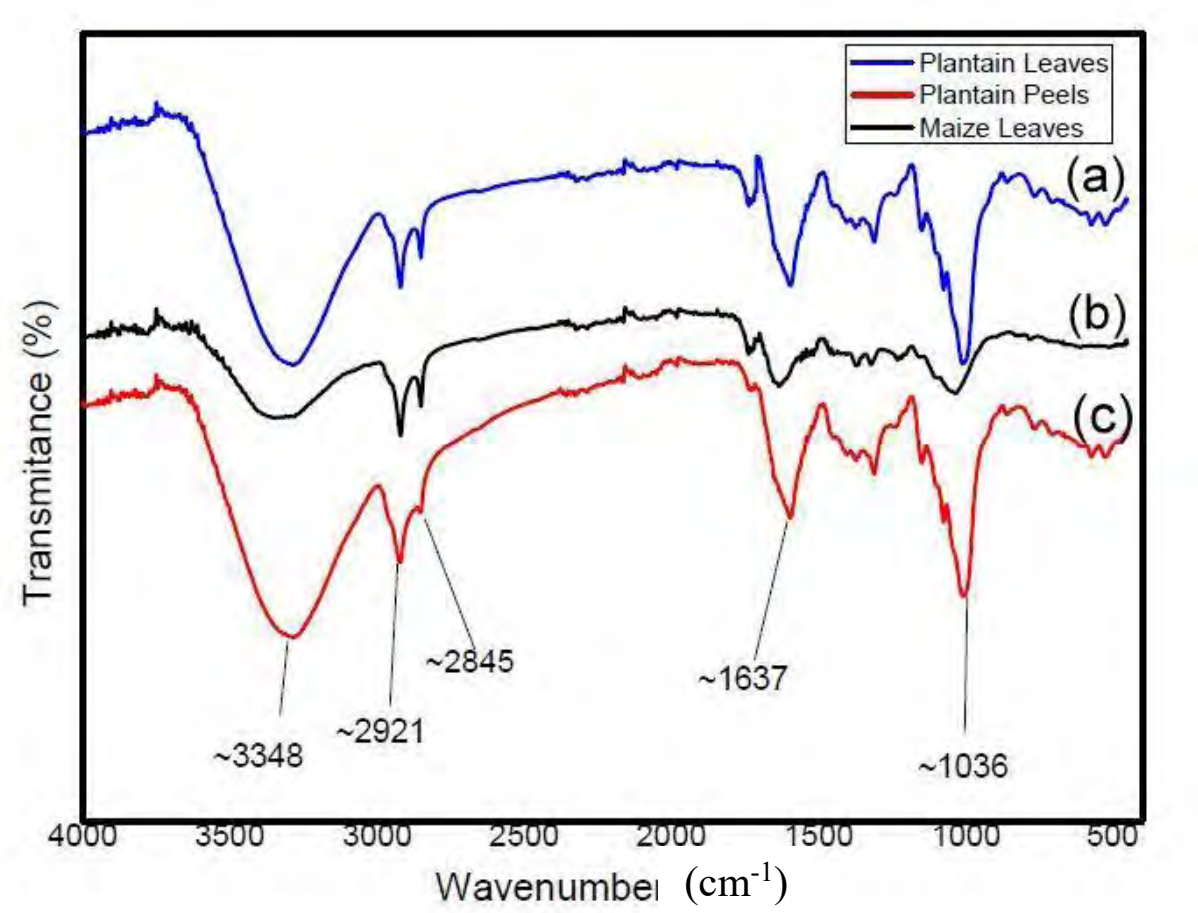

Figure 4. 2 FTIR plot of extracts used in the synthesis (a) Plantain leaves (b) Maize leaves (c) Plantain peels

Absorbance bands of the synthesized Fe_3O_4-NPs were observed at ~3340, ~1640, ~1063, ~900 and ~544 cm^{-1}. The reduction in the intensity of band 3500 – 3214 cm^{-1} in the extracts shows the involvement of the phenol compounds in the reduction of the Ferrous and ferric chloride precursors. Based on the reduction in band intensities at ~1637 and ~1036 cm^{-1}, proteins are also involved in the reduction of the Ferrous and ferric chloride precursors. The presence of the peak at ~544 cm^{-1} correspond to stretching vibrations of Fe-O bonds depicting the presence of Fe_3O_4 [73].

The FTIR results, shown in Figures 4.3 to Figure 4.5, all make evident that the soluble elements present in the maize leaves, plantain peels and plantain leaves extracts could have been

reducing and stabilizing agents in the synthesis process. The proteins and phenol compounds are believed to have been involved in the formation of Fe_3O_4.

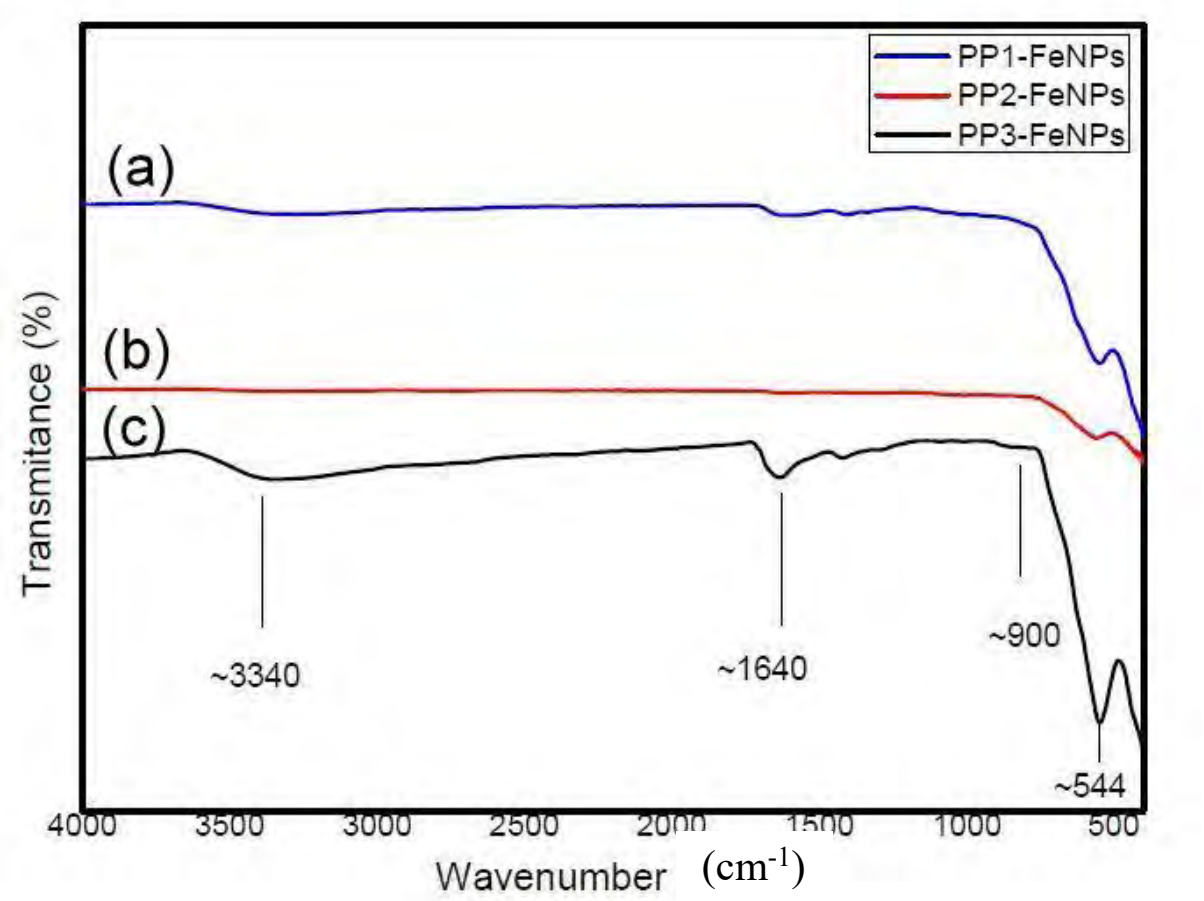

Figure 4. 3 FTIR of plantain peels synthesised nanoparticles (a) PP1-FeNP (b) PP2-FeNP (c) PP3-FeNP

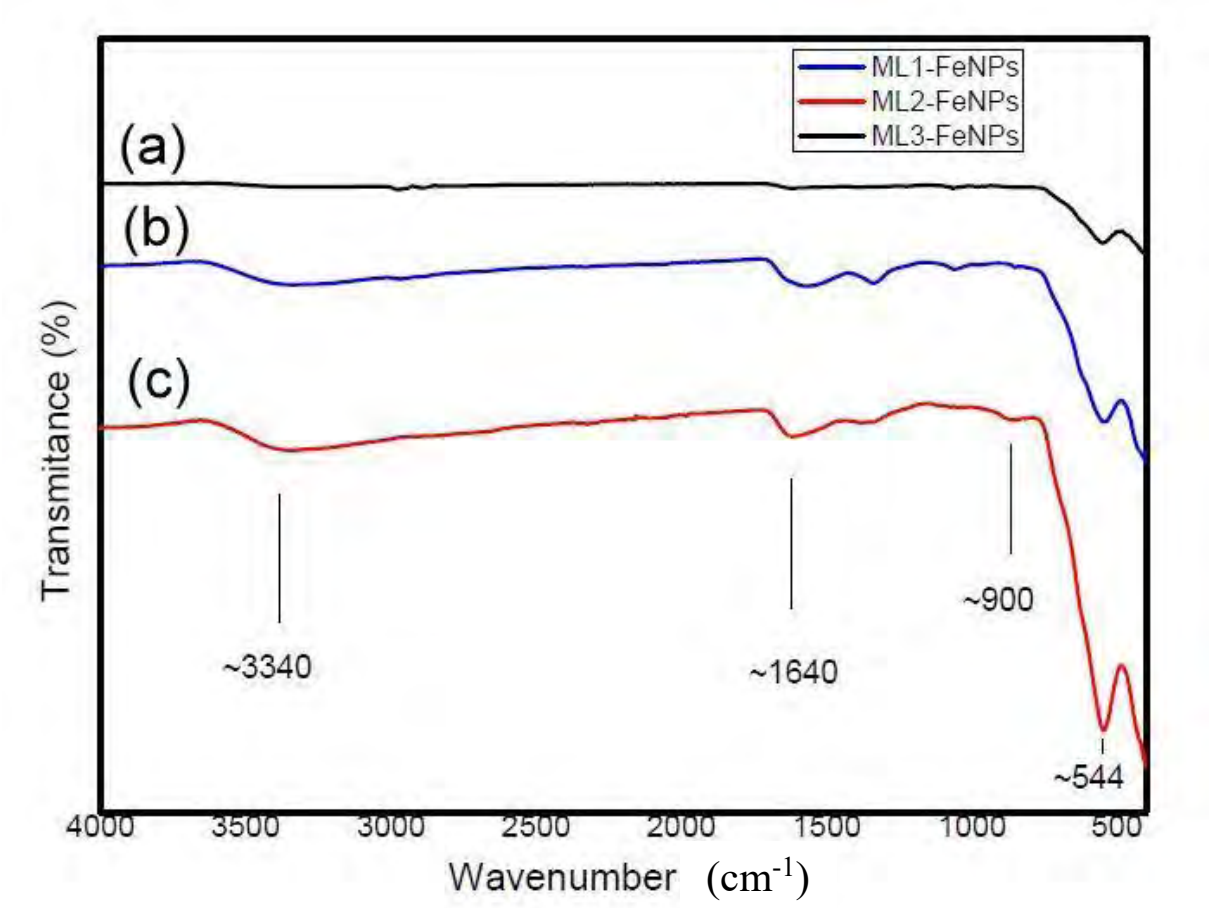

Figure 4. 4 FTIR of Maize leaves synthesised nanoparticles (a) ML1-FeNP (b) ML2-FeNP (c) ML3-FeNP

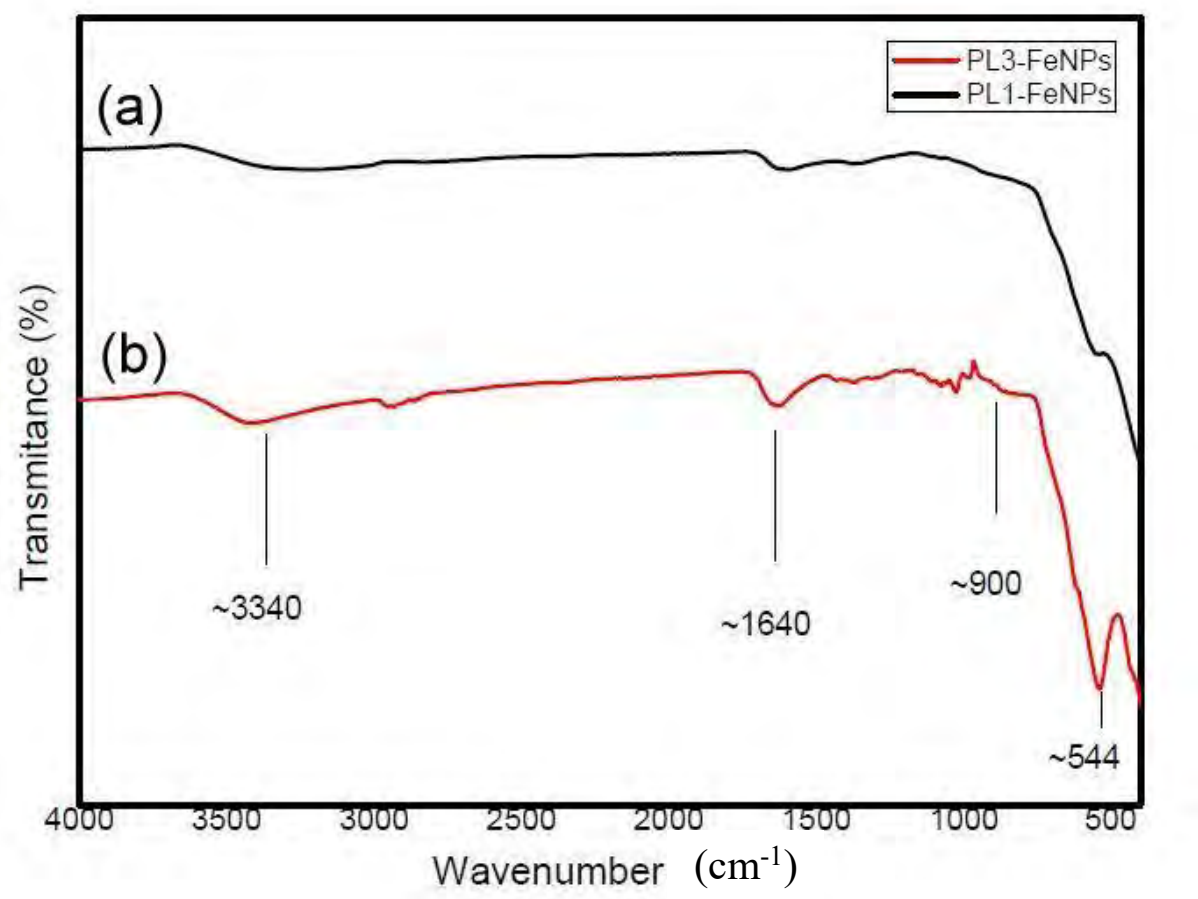

Figure 4. 5 FTIR of Plantain leaves synthesised nanoparticles (a) PL1-FeNP (b) PL2-FeNP (c) PL3-FeNP

4.3. X-Ray Diffraction (XRD)

Fe_3O_4-NPs were characterized by X-ray powder diffraction and patterns were collected to identify phases and crystalline structure. In total, it was found that there were intense diffraction peaks indexed (220), (311), (400), (422), (511), (440) and (533) at 2 theta values of 30.1°, 35.5°, 43.1°,54.5°, 57.6°, 62.8° and 74.2° respectively. The standard XRD data for magnetic iron oxide having a face-centered cubic structure was similar to the recorded data. The different molar ratios of the Fe^{3+} and Fe^{2+} used in the synthesis affected the XRD data obtained.

All the above index at their appropriate 2 theta values are seen in the Molar ratio 2 and 3 but absent in the molar ratio 1.

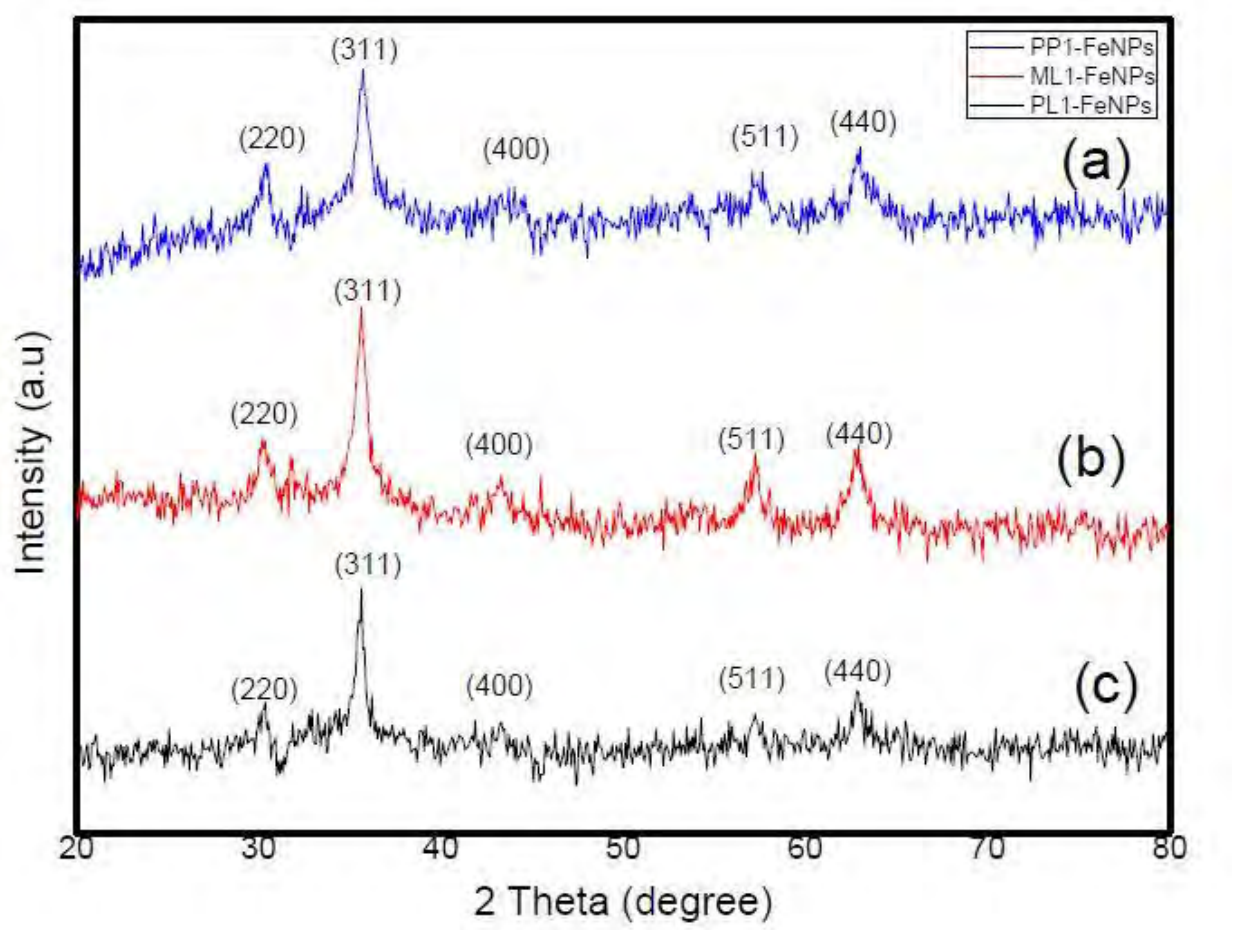

Figure 4. 6 XRD pattern of Fe_3O_4 MNPs synthesised with molar ratio 2:1 (a) PP1-FePs (b) ML1-FePs (c) PL1-FePs

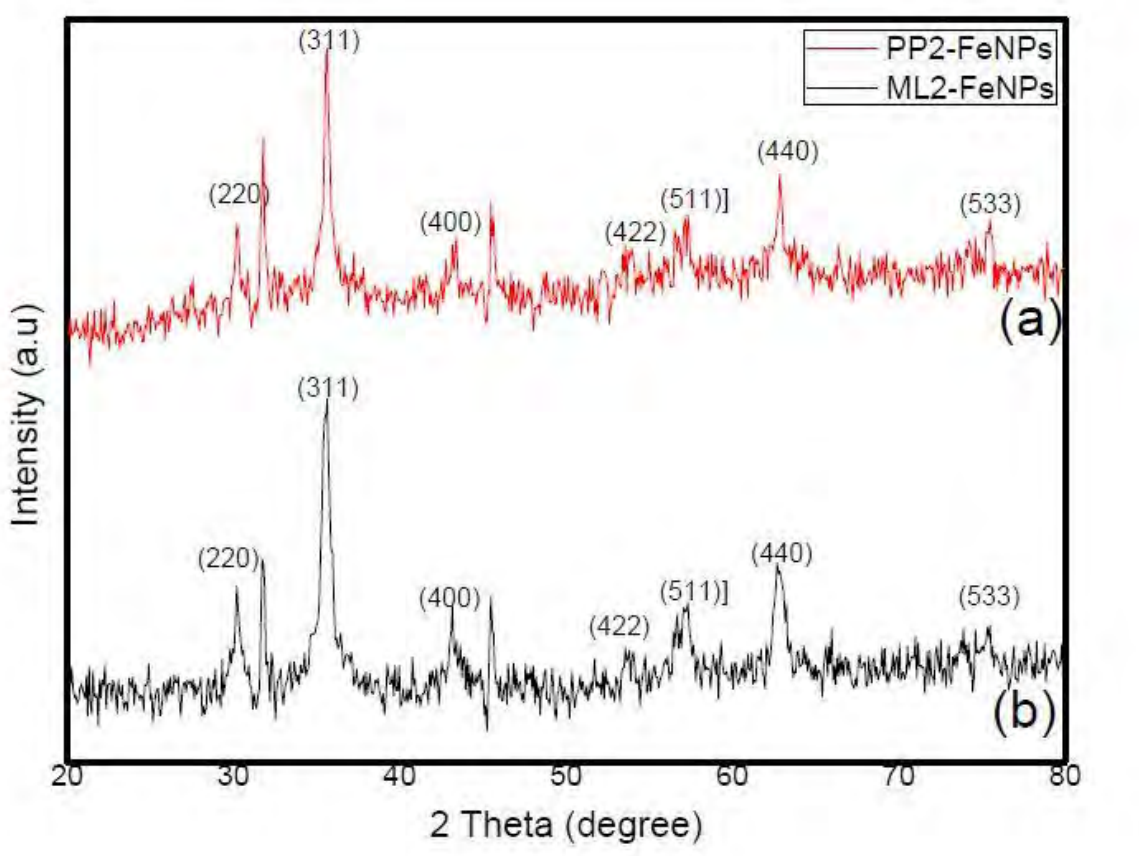

Figure 4. 7 XRD pattern of Fe_3O_4 MNPs synthesized with molar ratio 2:2 (at higher concentration). (a) PP2-FePs (b) ML2-FePs

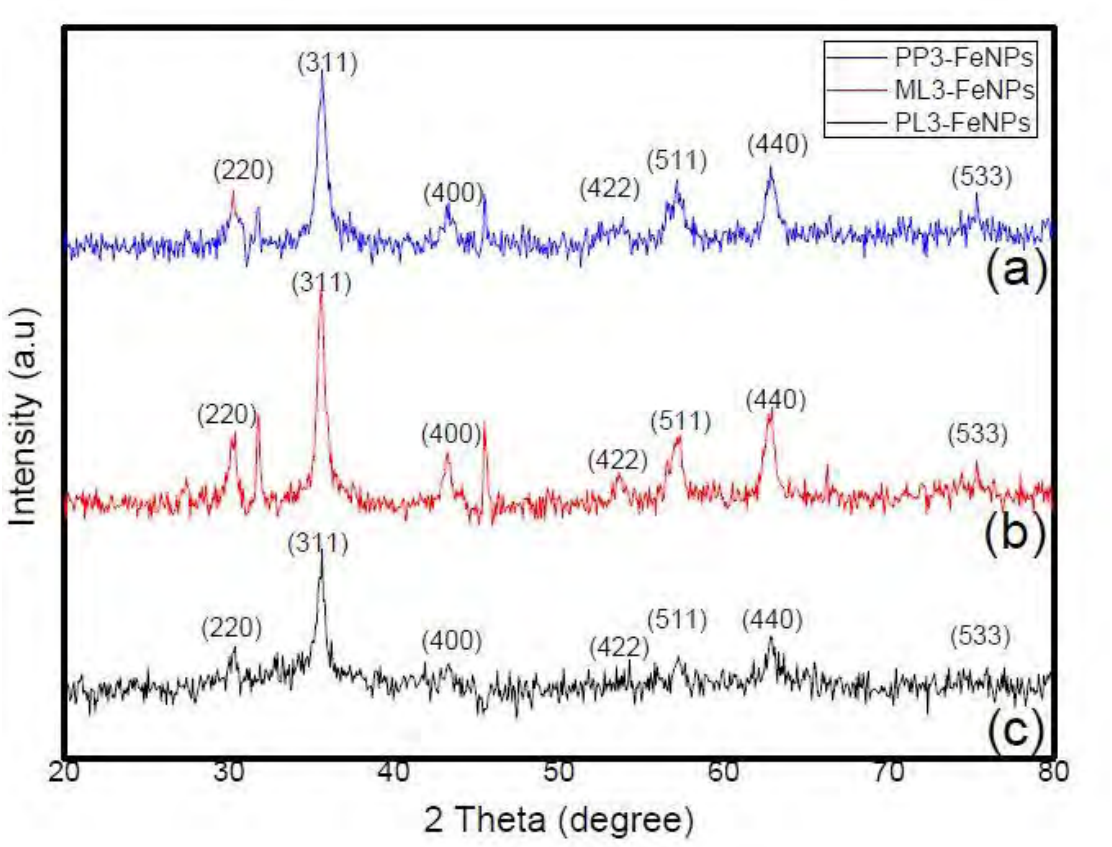

Figure 4. 8 XRD pattern of Fe_3O_4 MNPs synthesised with molar ratio 2:1 with increased concentration (a) PP3-FePs (b) ML3-FePs (c) PL3-FePs

With the aid of the Debye-Scherrer relation, crystallite sizes were estimated.

$$D = \frac{0.89\lambda}{\beta\, Cos\, \theta}$$

With

D representing the average crystallite size,

λ representing the wavelength of the Cu-Kα irradiation,

β represent FWHM of the most intense of the peak

θ represents the diffraction angle of the (311) peak of the magnetic Fe_3O_4 NPs

Table 4. 1 Sample and their Crystallite Size

Sample	FWHM (β)	Peak Position	Crystallite Size (nm)
ML1-FePs	1.23489	35.59	7.05
ML2-FePs	0.67849	35.56	12.84
ML3-FePs	0.62413	35.56	13.96
PL1-FePs	0.88249	35.72	9.87
PL3-FePs	0.87617	35.55	9.94
PP1-FePs	1.08648	35.72	8.02
PP2-FePs	0.4509	35.61	19.34
PP3-FePs	0.71084	35.63	12.26

From the crystallite size calculated from the XRD data, shown in Table 4.1 above, it can be concluded that for the all synthesis with the extracts done, when the concentration of the precursor (Fe^{3+} and Fe^{2+}) used increased, the crystallite size increased too.

It can be observed that the crystallite sizes of the plantain Leaves synthesized Fe_3O_4 NPs are larger compared with those of the plantain peels, the plantain peels', larger than those of the maize leaves.

An appreciable increase in the crystallite size is observed when the molar ratio or the precursors is brought to 2:2 but of higher concentration. An increase in the concentration of the molar ratio 2:1 causes a great increase in the crystallite size.

4.4. Energy Dispersive X-Ray (EDX)

The EDX data obtained from the synthesized particles suggested in most of the particles formed, there were other elements besides Fe and O, mostly Na and Cl which also was evident in XRD by the display of peaks around 2 theta angles of 32° and 45.5 ° (found in Figure 4.6, Figure 4.7 and Figure 4.8). The presence of these was considered possible with the Na emanating for the NaOH alkaline and Cl from the Iron salts, all used in the synthesis. The EDX data shown in Figure 4.9 – Figure 4. 16, display the presence of other elements, thus Calcium, Silicon, magnesium and Potassium, which shows the complexity of the plant extracts. Na, Ca, K, Si and Mn may be responsible for the capping of the particles.

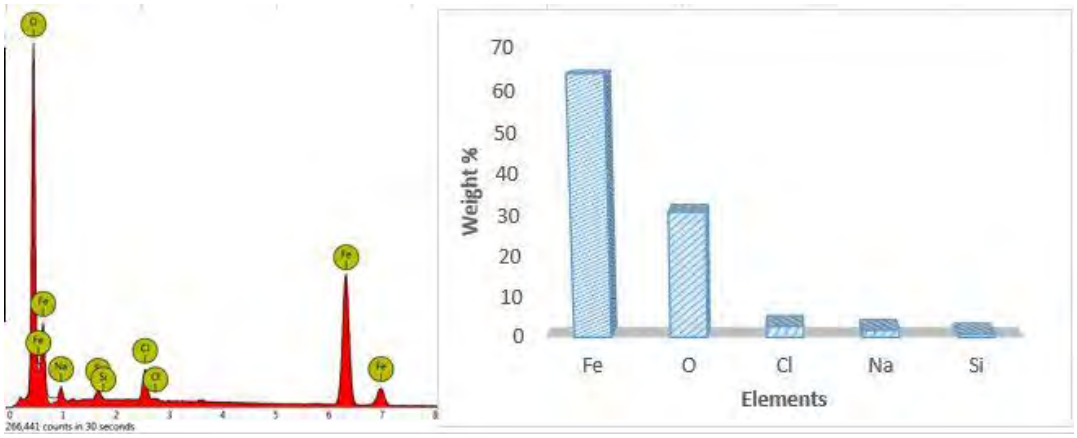

Figure 4. 9 EDX spectra (a) ML1-FePs (b)% of constituent elements found

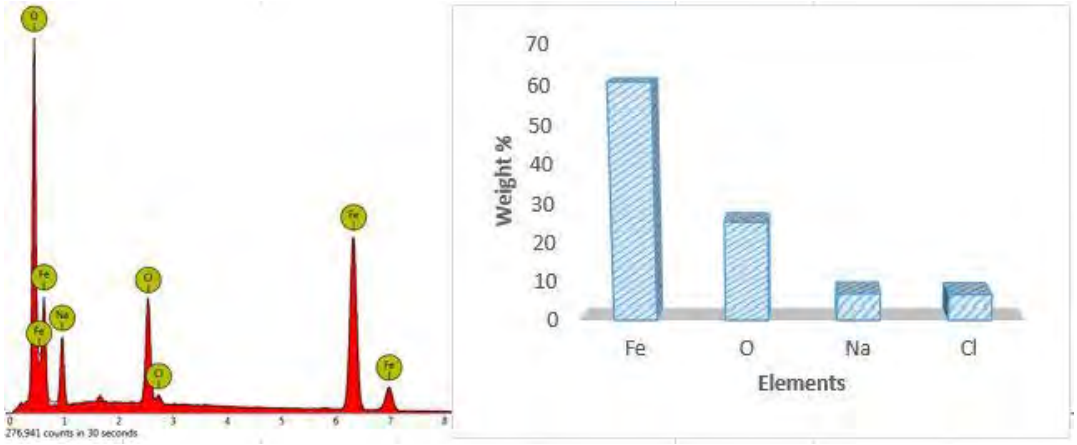

Figure 4. 10 EDX spectra (a) ML-FePs (b)% of constituent elements found

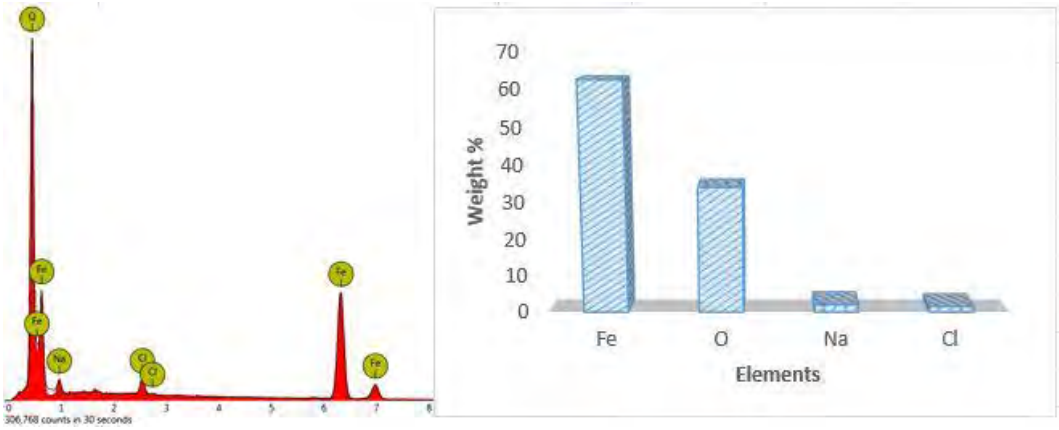

Figure 4. 11 EDX spectra (a) ML3-FePs (b)% of constituent elements found

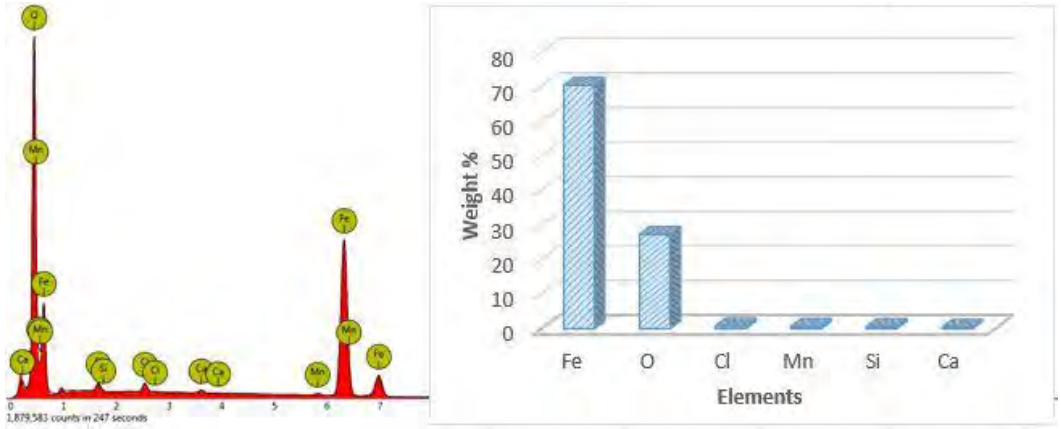

Figure 4. 12 EDX spectra (a) PL1-FePs (b)% of constituent elements found

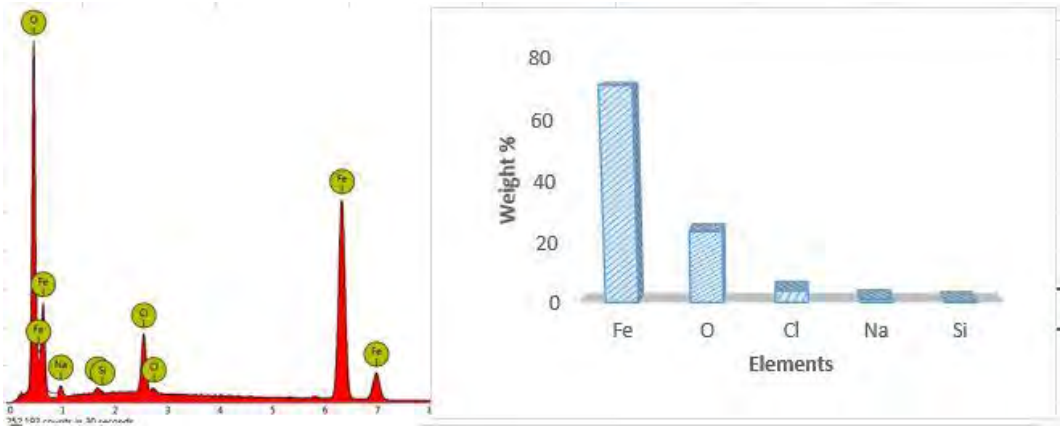

Figure 4. 13 EDX spectra (a) PL3-FePs (b)% of constituent elements found

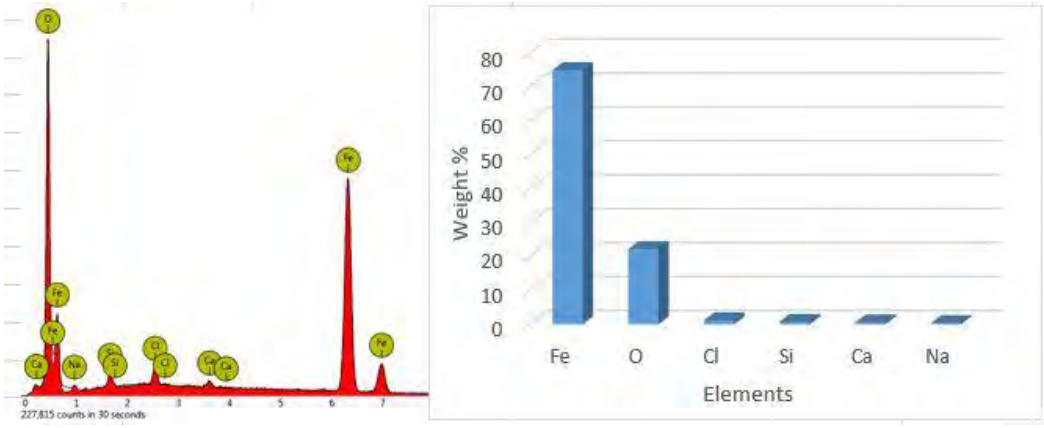

Figure 4. 14 EDX spectra (a) PP1-FePs (b)% of constituent elements found

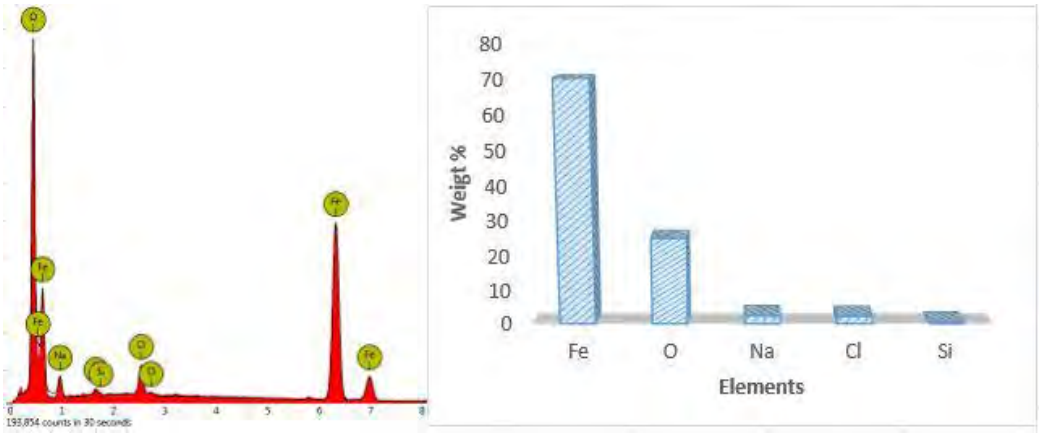

Figure 4. 15 EDX spectra (a) PP2-FePs (b)% of constituent elements found

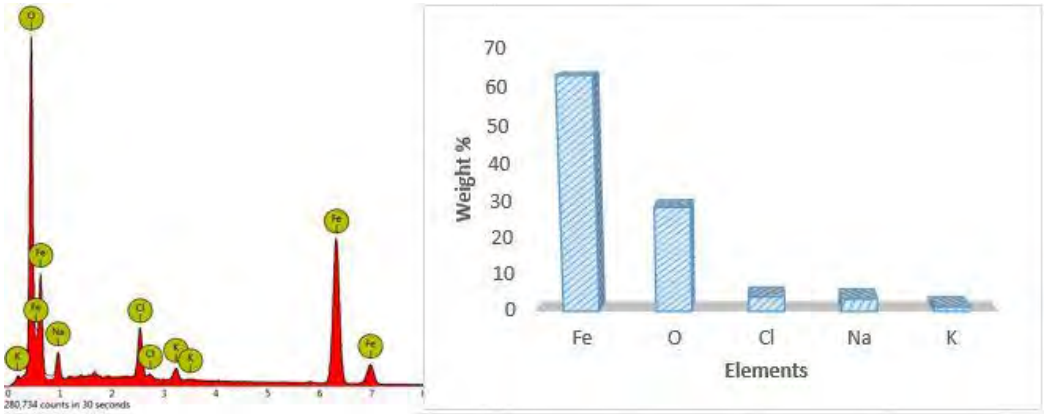

Figure 4. 16 EDX spectra (a) PP3-FePs (b)% of constituent elements found

4.5. Scanning Electron microscope

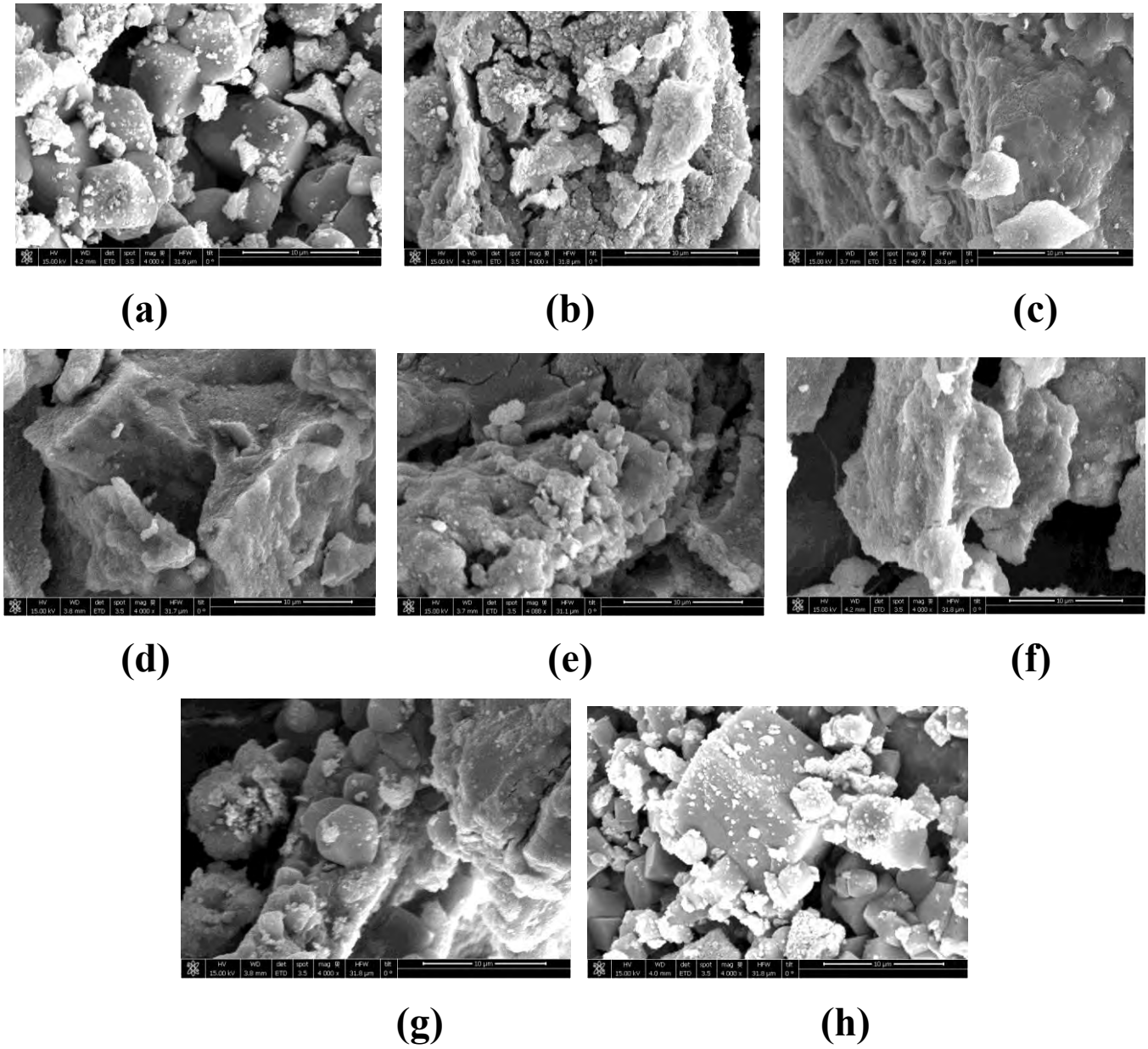

Figure 4. 17 SEM of samples at X4000 magnification (a) ML1-FePs (b) ML2-FePs (c) ML3-FePs (d) PL1-FePs (e) PL3-FePs (f) PP1-FePs (g) PP2-FePs (h) PP3-FePs.

The images collected from the Scanning electron microscope (SEM) are shown in Figure 4.17 above. The images display various size and shapes of particles within the samples scanned. Table 4.2 below shows the shapes observed and their sizes observed in Figure 4.17 above.

Table 4. 2 Table of samples and their shapes and sizes shown in SEM images

Sample	Observed shapes/ structure	Sizes
(a) ML1-FePs	Cubic and spherical	0.25 µm – 4.7 µm
(b) ML2-FePs	Spherical and irregular	0.23 µm – 8.2 µm
(c) ML3-FePs	Spherical and irregular	0.21 µm - 8.6 µm
(d) PL1-FePs	Irregular	0.54 µm- 6.1 µm
(e) PL3-FePs	Spherical and irregular	1.03µm- 4.3 µm
(f) PP1-FePs	Irregular	0.58 µm- 0.66 µm
(g) PP2-FePs	Spherical and irregular	0.25 µm- 4.75 µm
(h) PP3-FePs	Cubic and spherical	0.33 µm- 2.19 µm

The irregularity and largeness of the particles in Figure 4.17 (e) can be attributed to the ineffectiveness of the capping agent present in the plant extracts. It can be considered as high levels of agglomeration which have been reported in many literatures as one of the flaws of some biosynthesis methods.

4.6. CV analysis and Cell Viability

Figure 4.19 – 4.22 show the CV results for the blank and Fe_3O_4 particles after their 30, 60 and 90 min interaction with the Hela cells. The anodic peak currents were used to determine the ion exchange between the cell intracellular medium and the extracellular medium. The CV revealed the outflow of ions into the extracellular medium (indicated by a higher anodic current) and an inflow of ions into the intracellular medium (indicated by a low anodic current).

The rise and fall of the anodic currents specifies polarization and depolarization of the Hela cell membrane respectively.

Figure 4.19 describes the effect of the particles on the Hela cells upon addition 5 μL concentration.. The plot shows that the anodic currents of ML3-FePs, PP2-FePs and ML2-FePs fell below that of the Hela cell, indicating polarization. Literature reports that cancer cells generating signal for proliferation process using depolarization [120]. This indicates that the particles could promote proliferation in the Hela cell at a concentration of 5 μL. PL3-FePs triggered polarization, as its recorded an anodic current slightly above that of the Hela cells. The anodic current of PL1-FePs, PP1-FePs, PP3-FePs and ML1-FePs were extremely above that of the cells and this is a suggestive of hyperpolarization (when the intracellular medium becomes more negative). Since cancer proliferation signals are generated through depolarization, the hyperpolarization recorded by the particles is indicative of inhibition of the proliferation signals. PL1-FePs, PP1-FePs, PP3-FePs and ML1-FePs did not contribute to the ion flow of the Hela cells at this concentration.

Addition of 10 μL of the particles are yielded Figure 4.20. ML3-FePs and PP3-FePs showed similar trend as PL1-FePs, PP1-FePs, PP3-FePs and ML1-FePs shown at 5 μL. PL3-FePs polarized the Hela cells whereas PP2-FePs, ML1-FePs, PP1-FePs, PL1-FePs and ML2-FePs produced a hyperpolarization, with ion outflow highest in PP2-FePs

Figure 4.21 showed the currents against Voltage when the 15 μL was added to the cells. It reveals that after the addition pf 15 μL, ML3-FePs, PP2-FePs, PL3-FePs and PP3-FePs triggered. ML1-FePs, PP1-FePs, PL1-FePs and ML2-FePs gave polarization whereas PL1-FePs recorded higher anodic current hence triggering hyperpolarization.

Final addition of 20 μL of the particles to the Hela cells in Figure 4.22 indicates that PL1-FePs, ML3-FePs, PP3-FePs and ML2-FePs also did not contribute to the cell ion exchange. PP2-FePs

triggered a moderate outflow of ions, hence causing polarization. PL3-FePs on its addition showed higher efflux (hyperpolarization). PP2-FePs and ML1-FePs also displayed moderate outflow of ions.

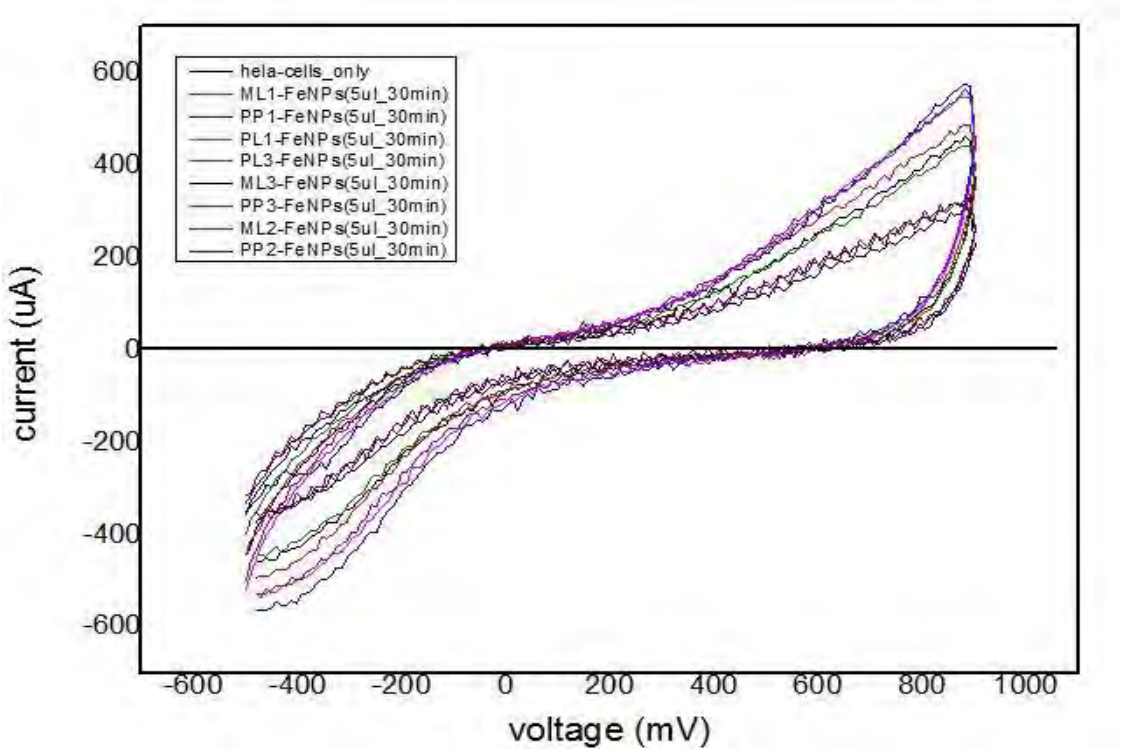

Figure 4. 18 CV analysis plot after 5µl of sample suspension was added.

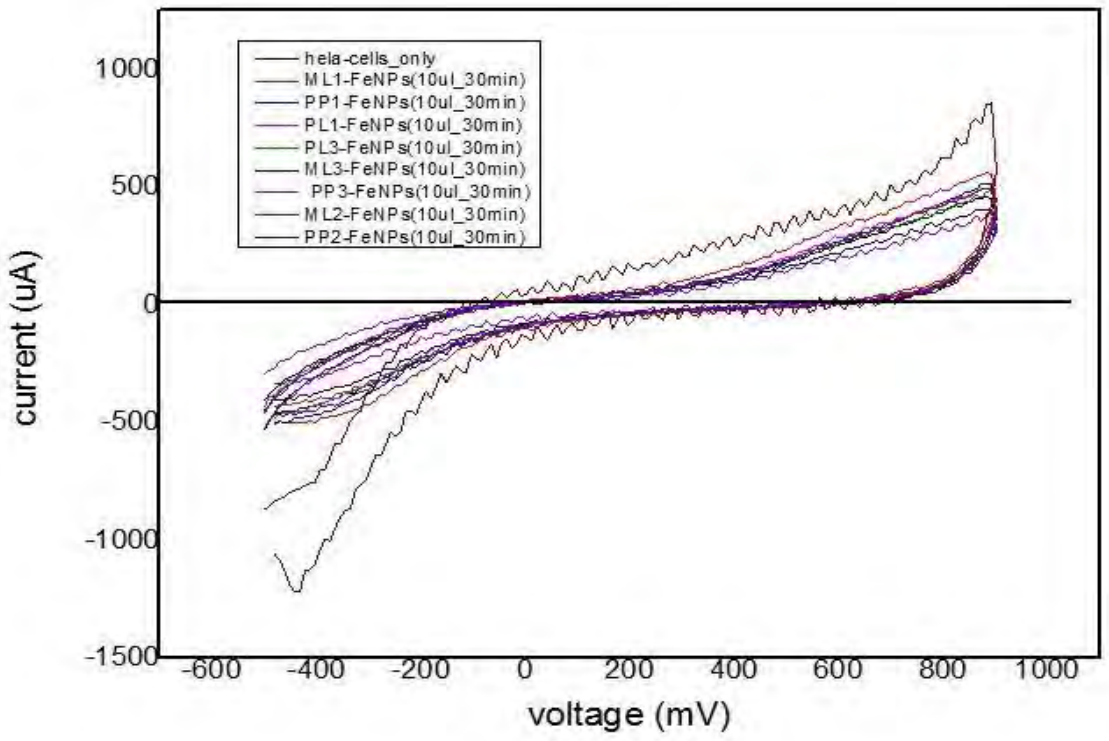

Figure 4. 19 CV analysis plot after 10µL of sample suspension was added.

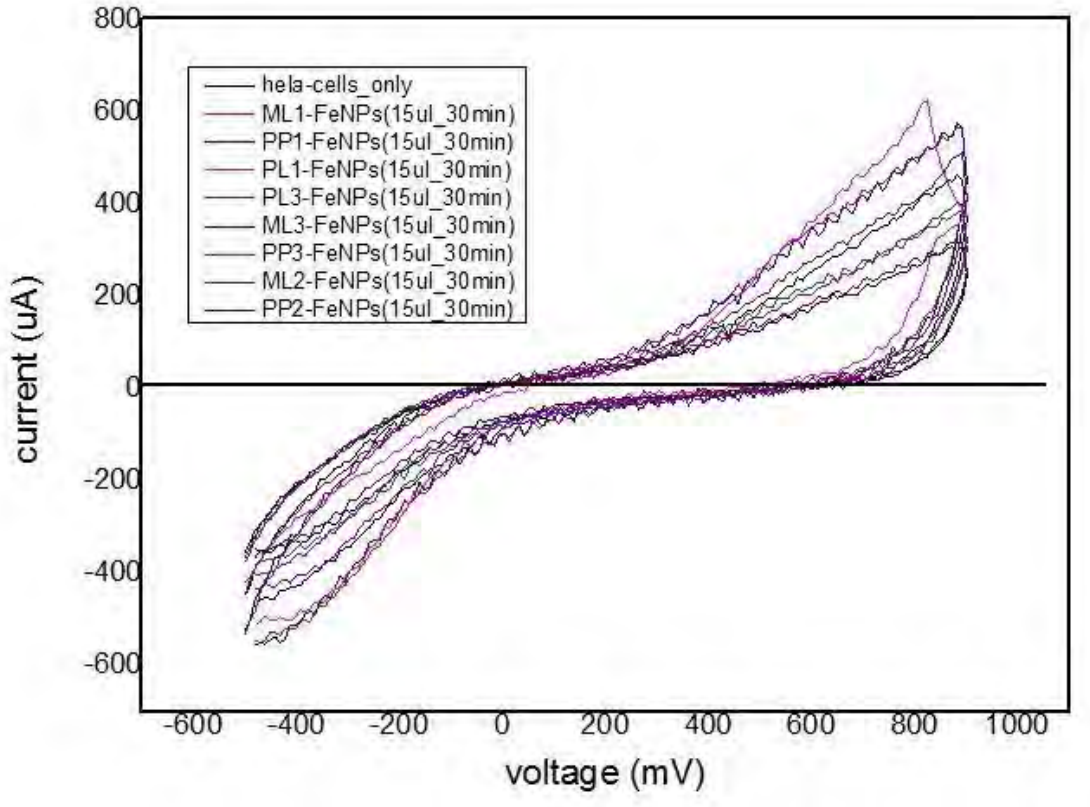

Figure 4. 20 CV analysis plot after 15µL of sample suspension was added.

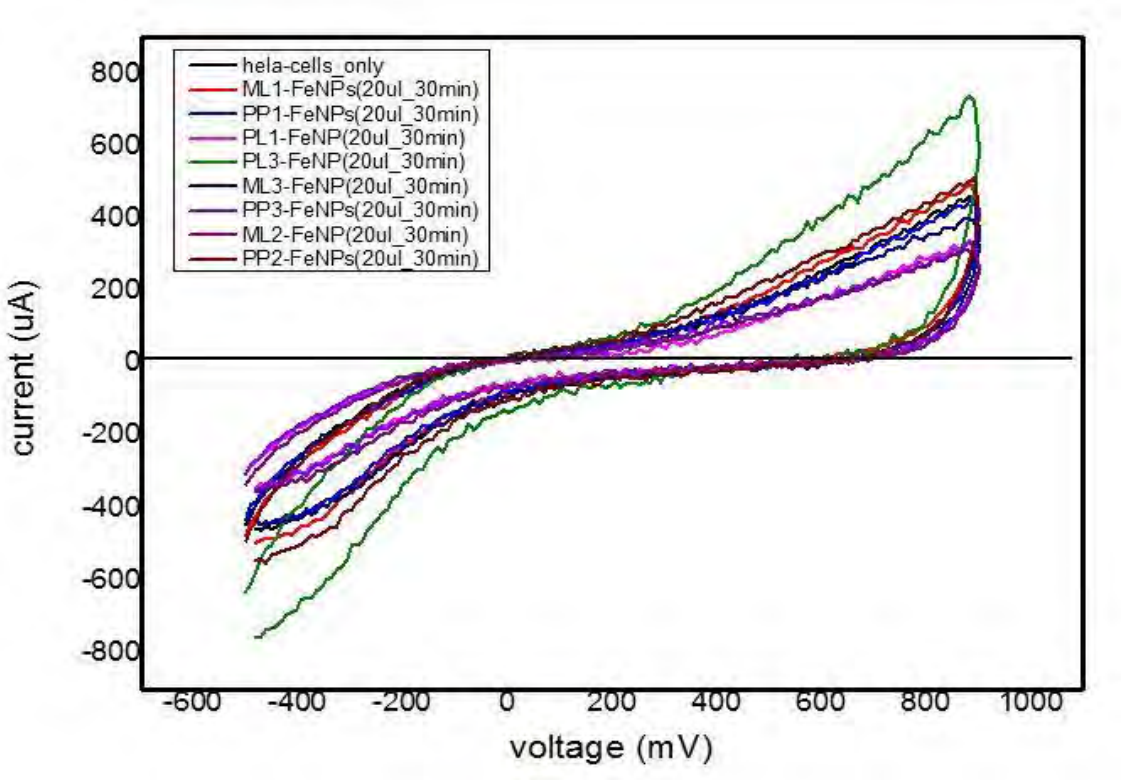

Figure 4. 21 CV analysis plot after 20 μL of sample suspension was added

Figure 4.23 to Figure 4.25 below, describe the variation of the anodic current with the total volumes of samples used. These relations were extracted from Figure 4.19 to Figure 4.22 above.

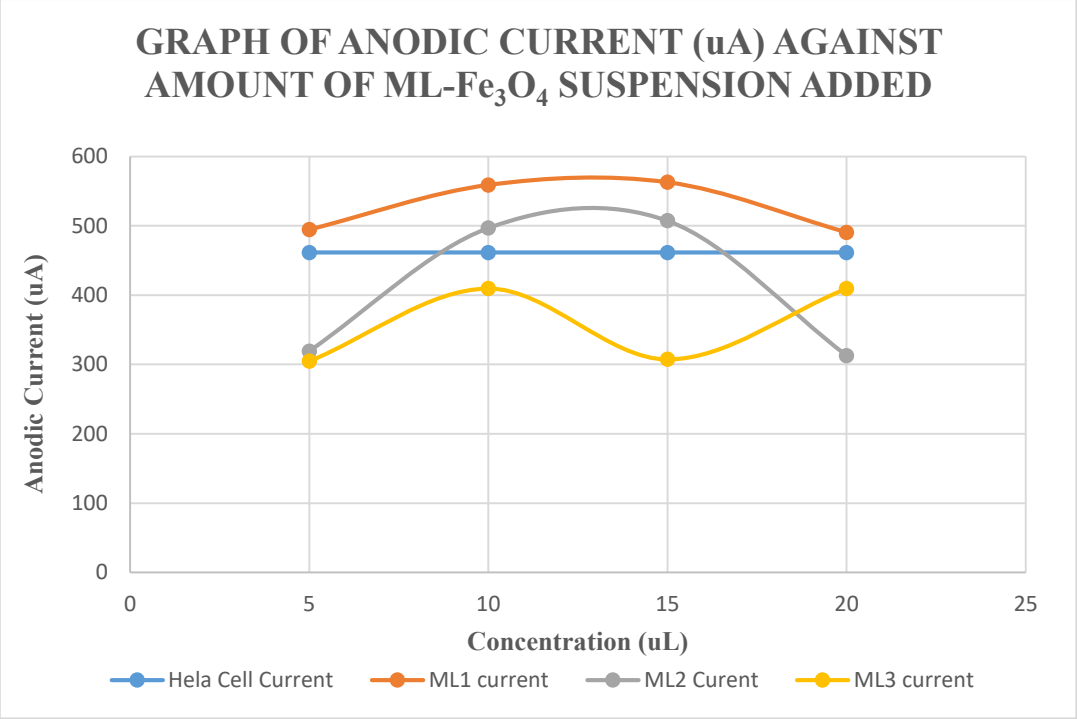

Figure 4. 22 Graph displaying the ion flow when ML-Fe_3O_4 NPs were employed

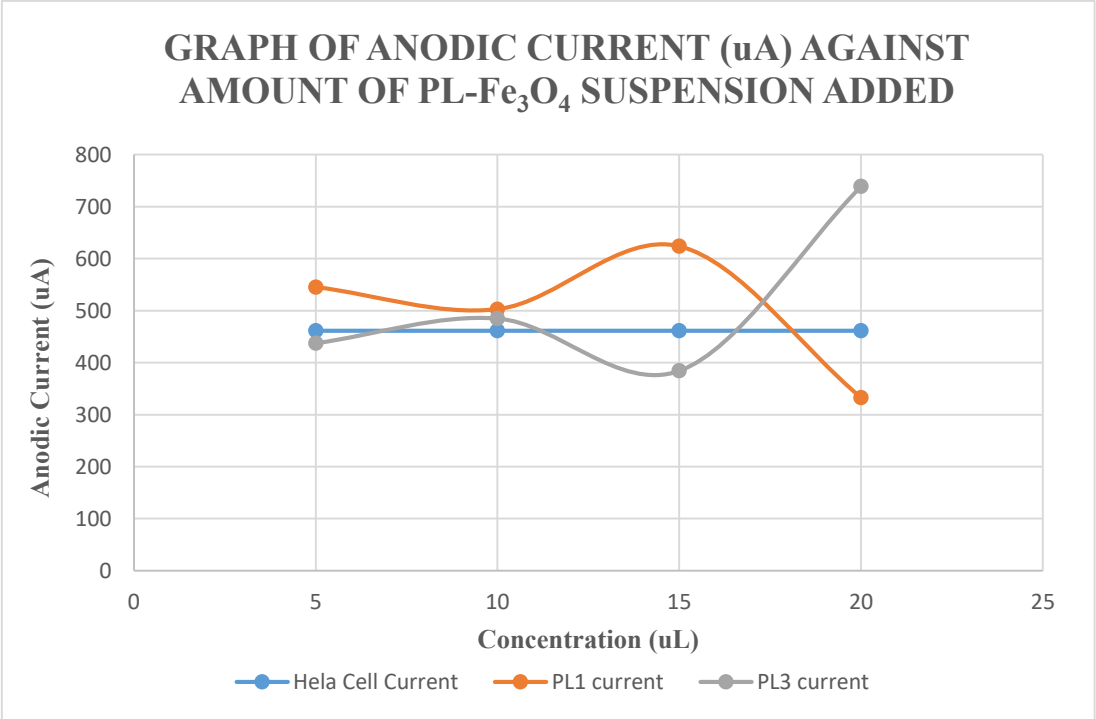

Figure 4. 23 Graph displaying the ion flow when PL-Fe_3O_4 NPs were employed

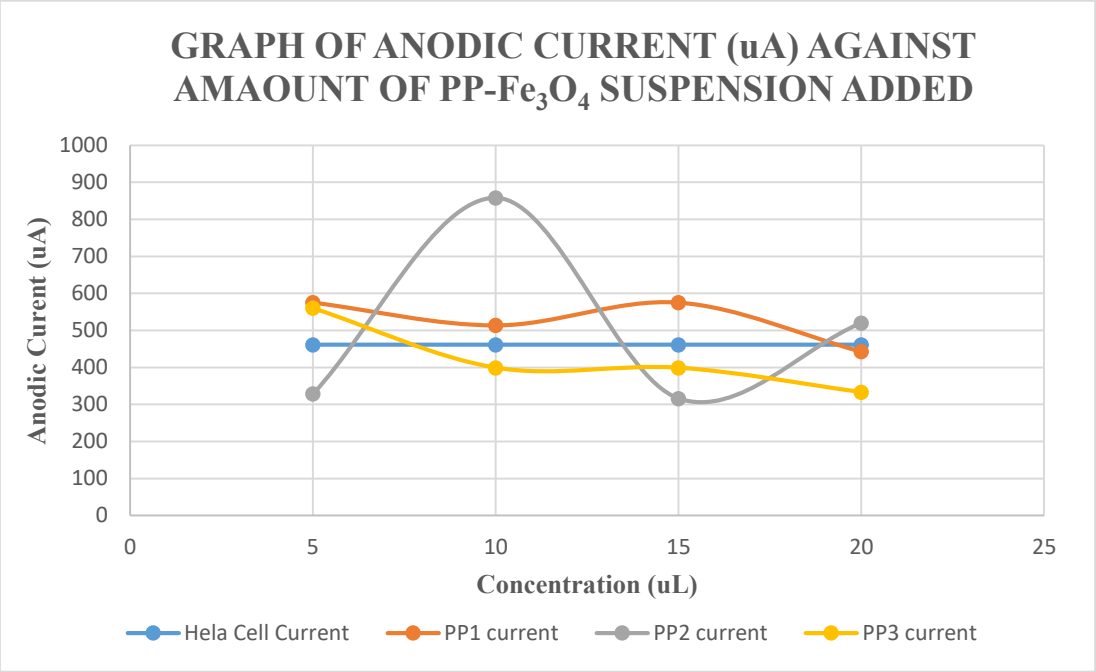

Figure 4. 24 Graph displaying the ion flow when PP- Fe_3O_4 NPs were employed

The table below summarises the anodic current response as depicted in Figures 4.23 – Figure 4.25.

Table 4. 3 Anodic responds relative to Hela cells.

Sample Name	5 μL	10 μL	15 μL	20 μL
ML1-FePs	+	++	++	+
ML2-FePs	-	+	+	-
ML3-FePs	-	-	-	-
PL1-FePs	+	+	++	-
PL3-FePs	-	+	-	++
PP1-FePs	+	+	+	-
PP2-FePs	-	++	-	+
PP3-FePs	+	-	-	-

In Table 4.3 above

(-) indicates Decreased Membrane Permeation/ no distraction of membranes

(+) indicate Moderate Membrane Permeation

(++) indicate Extreme or Enhanced Membrane Permeation

Figure 4.23 – 4.25 and Table 4.3, show the summary of the particle behaviour on the cells based on the extracts used. Among all the particle, ML1-FePs at 10 μL and 15 μL (Figure 4.23), PL1-FePs at 15 μL and PL3- FePs at 20 μL (Figure 4.24) and PP2-FePs at 5 μL (Figure 4.25) indicated hyperpolarization. The different behaviours of the Hela cells at different concentrations of the particles could point to particle sizes playing a role in their inhibitory work.

Table 4. 4 Samples and their corresponding Cell viability percentage

Sample Name	**Cell Viability %**
ML1-FePs	50.41
ML2-FePs	58.46
ML3-FePs	59.46
PL1-FePs	58.20
PL3-FePs	60.82
PP1-FePs	58.82
PP2-FePs	59.05
PP3-FePs	58.16

Table 4.4, reveals the possible contribution of the particles to a reduction in cell viability in accordance to a possible proliferation inhibitory action as suggested by the CV information.

This may support the report of Patra et al. on proteasmal inhibition by Fe_3O_4 in cancer treatment [12].

CHAPTER FIVE

5.0. CONCLUSION AND RECOMMENDATION

5.1. Conclusion

The novelty in the green synthesis of iron oxide particles using Maize leave blade. Plantain leaves and peels were also used to synthesis magnetic particles. Farm produce wastes which are non-hazardous and easy to dispose of, can perform reducing, stabilizing and capping roles in this synthesis and was the reason for their use. The synthesized Fe_3O_4–NPs (PPeels Fe_3O_4NPs, PLeaves Fe_3O_4NPs and MLeaves Fe_3O_4NPs) were analyzed by FT-IR, UV-Vis Spectroscopy, XRD, CV, EDX and SEM.

The UV-Vis was conducted to confirm the formation of the Fe_3O_4 in the synthesis process. The UV-Vis spectroscopy spectra of the particles displaced absorbance within 300-800 nm wavelength range which is in agreement with literature for the production of the magnetic iron oxide nanoparticles.

The EDX was conducted to confirm the formation of the Fe_3O_4 by checking for presence of Iron (Fe) and Oxygen (O) in the sample. EDX data proved the existence of iron (Fe) and oxygen (O) in the produced particles. In addition, it showed the presence of other elements which include Silicon (Si), sodium (Na), Magnesium (Mn), Calcium (Ca) and Potassium (K). The presence of these other elements found in the particles was attributed to the elemental complexity of the plant extracts employed during the synthesis.

The FTIR was conducted to confirm the presence of the Fe-O to indicate the formation of the Iron oxide being synthesised. The FTIR spectra obtained for the plants and the resulting particles produced, all pointed to the involvement of proteins and phenol compound from the plant in the synthesis of the particles. They displaced a reduction in the –OH, N-H and C-N

bands led to the conclusion of the proteins and phenols in the production of the Fe_3O_4 as hypothesized.

In the XRD data obtained from the synthesised particles, intense diffraction peaks indexed (220), (311), (400), (422), (511), (440) and (533) at 2theta values of 30.1°, 35.5°, 43.1°,54.5°, 57.6°, 62.8° and 74.2° respectively. This tally with the standard XRD data for magnetic iron oxide with face-centered cubic structure. After the calculation of the crystallite sizes of the particles was done using the Debye-Scherrer relation, it showed that increasing the concentration of the iron chloride precursors used resulted in an increment in the crystallite sizes of the particles produced. It was also observed that the crystallite sizes of PLeaves Fe_3O_4NPs were found to be greater than PPeels Fe_3O_4NPs and they also greater compare with MLeaves Fe_3O_4NPs, all at a common concentration. The crystallite size of PL1-FePs (9.87 nm) was greater than PP1-FePs (8.02 nm) and that also greater than ML1-FePs (7.05 nm). At a common molar ratio, an increase in concentration resulted in an increase in crystallite size in both PL2-FePs (from 7.05nm to 12.84 nm) and ML2-FePs (from 8.02nm to 19.34 nm). Changing of the molar ratio to 2:2 and increasing of the concentration of precursors resulted in crystallite size increase (thus, comparing ML3-FePs, PL3-FePs and PP3-FePs to ML1-FePs, PL1-FePs and PP1-FePs).

SEM images revealed high levels of particles agglomeration. It was suspected to be as a result of the failure of most of the capping agents in the plant extracts employed during the synthesis process. Some of the particles showed very high levels of agglomeration compared with others. The morphology of the particles cannot be clearly defined in most of the samples due to this.

All particles synthesized exhibited potential threatening effects to Cancer cell recording a reduction in the Hela cell viability (50.41- 60.82). The effect of the particles at different

concentration, on the Hela cells varied. A speculation is that; the particle sizes could be contributing to the reduction in the viability of the Hela cells.

5.2. Recommendations

1) Further research could be conducted to explain the exact mechanism of cell death.
2) The effect of the volume of precursors on the crystallite size of the NP should be investigated.
3) The synthesized NPs should be tested on other Cells.
4) Future work must could be done to investigate the effect of the Fe_3O_4 particle size on Cancer cells.

REFERENCES

1. Organization, W.H. *Cancer. 2015*. World Health Organization. Available in http://www. who. int/mediacentre/factsheets/fs297/en.[Links] 2016 [cited 2018 June 22]; Available from: http://www.who.int/mediacentre/factsheets/fs297/en.
2. Bharali, D.J. and S.A. Mousa, *Emerging nanomedicines for early cancer detection and improved treatment: current perspective and future promise.* Pharmacology & therapeutics, 2010. **128**(2): p. 324-335.
3. Zhang, J., et al., *Lyophilized paclitaxel magnetoliposomes as a potential drug delivery system for breast carcinoma via parenteral administration: in vitro and in vivo studies.* Pharmaceutical research, 2005. **22**(4): p. 573-583.
4. Oh, J., et al., *Magneto-motive detection of tissue-based macrophages by differential phase optical coherence tomography.* Lasers in surgery and medicine, 2007. **39**(3): p. 266-272.
5. Teja, A.S. and P.-Y. Koh, *Synthesis, properties, and applications of magnetic iron oxide nanoparticles.* Progress in crystal growth and characterization of materials, 2009. **55**(1-2): p. 22-45.
6. Wang, X., *Preparation of magnetic hydroxyapatite and their use as recyclable adsorbent for phenol in wastewater.* Clean–Soil, Air, Water, 2011. **39**(1): p. 13-20.
7. Xu, B., et al., *"Two-in-One" fabrication of Fe_3O_4/MePEG-PLA composite nanocapsules as a potential ultrasonic/MRI dual contrast agent.* Langmuir, 2011. **27**(19): p. 12134-12142.
8. Chen, X., et al., *Magnetic silica nanotubes: synthesis, drug release, and feasibility for magnetic hyperthermia.* ACS applied materials & interfaces, 2012. **4**(4): p. 2303-2309.

9. Jassal, V., U. Shanker, and S. Gahlot, *Green synthesis of some iron oxide nanoparticles and their interaction with 2-Amino, 3-Amino and 4-Aminopyridines.* Materials Today: Proceedings, 2016. **3**(6): p. 1874-1882.

10. Arum, Y., et al., *Chitosan-coated Fe_3O_4 magnetic nanoparticles as carrier of cisplatin for drug delivery.* Fisheries and aquatic sciences, 2015. **18**(1): p. 89-98.

11. Jayanthi, S.A., et al., *A novel hydrothermal approach for synthesizing α- Fe_2O_3, γ-Fe_2O_3 and Fe_3O_4 mesoporous magnetic nanoparticles.* Materials Chemistry and Physics, 2015. **162**: p. 316-325.

12. Patra, J.K., et al., *Proteasome inhibitory, antioxidant, and synergistic antibacterial and anticandidal activity of green biosynthesized magnetic Fe_3O_4 nanoparticles using the aqueous extract of corn (Zea mays L.) ear leaves.* Artificial cells, nanomedicine, and biotechnology, 2017. **45**(2): p. 349-356.

13. Singh, P., et al., *Biological synthesis of nanoparticles from plants and microorganisms.* Trends in biotechnology, 2016. **34**(7): p. 588-599.

14. Khlebtsov, N. and L. Dykman, *Biodistribution and toxicity of engineered gold nanoparticles: a review of in vitro and in vivo studies.* Chemical Society Reviews, 2011. **40**(3): p. 1647-1671.

15. Jiao, H. and H. Yang, *Controlled synthesis and magnetic properties of Fe_3O_4 walnut spherical particles and octahedral microcrystals.* Science in China Series E: Technological Sciences, 2008. **51**(11): p. 1911-1920.

16. Wu, J.H., et al., *Sub 5 nm Fe_3O_4 nanocrystals via coprecipitation method.* Colloids and Surfaces A: Physicochemical and Engineering Aspects, 2008. **313**: p. 268-272.

17. Islam, M.N., J.-R. Jeong, and C. Kim, *A facile route to sonochemical synthesis of magnetic iron oxide (Fe_3O_4) nanoparticles.* Thin Solid Films, 2011. **519**(23): p. 8277-8279.

18. Seabra, A.B., P. Haddad, and N. Duran, *Biogenic synthesis of nanostructured iron compounds: applications and perspectives.* IET nanobiotechnology, 2013. **7**(3): p. 90-99.

19. Patra, J.K. and K.-H. Baek, *Green biosynthesis of magnetic iron oxide (Fe_3O_4) nanoparticles using the aqueous extracts of food processing wastes under photo-catalyzed condition and investigation of their antimicrobial and antioxidant activity.* Journal of Photochemistry and Photobiology B: Biology, 2017. **173**: p. 291-300.

20. Daniel-da-Silva, A.L., et al., *In situ synthesis of magnetite nanoparticles in carrageenan gels.* Biomacromolecules, 2007. **8**(8): p. 2350-2357.

21. Mohanpuria, P., N.K. Rana, and S.K. Yadav, *Biosynthesis of nanoparticles: technological concepts and future applications.* Journal of nanoparticle research, 2008. **10**(3): p. 507-517.

22. Rai, M., A. Yadav, and A. Gade, *CRC 675—current trends in phytosynthesis of metal nanoparticles.* Critical Reviews in Biotechnology, 2008. **28**(4): p. 277-284.

23. Cornell, R.M. and U. Schwertmann, *The iron oxides: structure, properties, reactions, occurrences and uses*. 2003: John Wiley & Sons.

24. Wu, W., et al., *Recent progress on magnetic iron oxide nanoparticles: synthesis, surface functional strategies and biomedical applications.* Science and technology of advanced materials, 2015. **16**(2): p. 023501.

25. Wu, W., et al., *Large-scale and controlled synthesis of iron oxide magnetic short nanotubes: shape evolution, growth mechanism, and magnetic properties.* The Journal of Physical Chemistry C, 2010. **114**(39): p. 16092-16103.

26. Majewski, P. and B. Thierry, *Functionalized magnetite nanoparticles—synthesis, properties, and bio-applications.* Critical Reviews in Solid State and Materials Sciences, 2007. **32**(3-4): p. 203-215.

27. Boxall, C., G. Kelsall, and Z. Zhang, *Photoelectrophoresis of colloidal iron oxides. Part 2.—Magnetite (Fe_3O_4).* Journal of the Chemical Society, Faraday Transactions, 1996. **92**(5): p. 791-802.

28. Thakkar, K.N., S.S. Mhatre, and R.Y. Parikh, *Biological synthesis of metallic nanoparticles.* Nanomedicine: Nanotechnology, Biology and Medicine, 2010. **6**(2): p. 257-262.

29. Cabrera, L., et al., *Magnetite nanoparticles: electrochemical synthesis and characterization.* Electrochimica Acta, 2008. **53**(8): p. 3436-3441.

30. Pascal, C., et al., *Electrochemical synthesis for the control of γ- Fe_2O_3 nanoparticle size. Morphology, microstructure, and magnetic behavior.* Chemistry of materials, 1999. **11**(1): p. 141-147.

31. Bomatí-Miguel, O., et al., *Calorimetric study of maghemite nanoparticles synthesized by laser-induced pyrolysis.* Chemistry of Materials, 2008. **20**(2): p. 591-598.

32. Bharde, A.A., et al., *Bacteria-mediated precursor-dependent biosynthesis of superparamagnetic iron oxide and iron sulfide nanoparticles.* Langmuir, 2008. **24**(11): p. 5787-5794.

33. Roh, Y., et al., *Extracellular synthesis of magnetite and metal-substituted magnetite nanoparticles.* Journal of nanoscience and nanotechnology, 2006. **6**(11): p. 3517-3520.

34. Blanco-Andujar, C., et al., *Elucidating the morphological and structural evolution of iron oxide nanoparticles formed by sodium carbonate in aqueous medium.* Journal of Materials Chemistry, 2012. **22**(25): p. 12498-12506.

35. Li, Z., et al., *Direct Coprecipitation Route to Monodisperse Dual-Functionalized Magnetic Iron Oxide Nanocrystals Without Size Selection.* small, 2008. **4**(2): p. 231-239.

36. Sun, S. and H. Zeng, *Size-controlled synthesis of magnetite nanoparticles.* Journal of the American Chemical Society, 2002. **124**(28): p. 8204-8205.

37. Liang, X., et al., *Synthesis of nearly monodisperse iron oxide and oxyhydroxide nanocrystals.* Advanced Functional Materials, 2006. **16**(14): p. 1805-1813.

38. Rockenberger, J., E.C. Scher, and A.P. Alivisatos, *A new nonhydrolytic single-precursor approach to surfactant-capped nanocrystals of transition metal oxides.* Journal of the American Chemical Society, 1999. **121**(49): p. 11595-11596.

39. Wang, Y., et al., *One-pot reaction to synthesize superparamagnetic iron oxide nanoparticles by adding phenol as reducing agent and stabilizer.* Journal of Nanoparticle Research, 2012. **14**(4): p. 755.

40. Woo, K., et al., *Easy synthesis and magnetic properties of iron oxide nanoparticles.* Chemistry of Materials, 2004. **16**(14): p. 2814-2818.

41. Bronstein, L.M., et al., *Influence of iron oleate complex structure on iron oxide nanoparticle formation.* Chemistry of materials, 2007. **19**(15): p. 3624-3632.

42. Hu, M., et al., *Hierarchical magnetic iron (III) oxides prepared by solid-state thermal decomposition of coordination polymers.* RSC Advances, 2012. **2**(11): p. 4782-4786.

43. Hu, M., J.-S. Jiang, and Y. Zeng, *Prussian blue microcrystals prepared by selective etching and their conversion to mesoporous magnetic iron (III) oxides.* Chemical Communications, 2010. **46**(7): p. 1133-1135.

44. Asuha, S., et al., *One step synthesis of maghemite nanoparticles by direct thermal decomposition of Fe–urea complex and their properties.* Journal of Alloys and Compounds, 2009. **472**(1-2): p. L23-L25.

45. Amara, D. and S. Margel, *Solventless thermal decomposition of ferrocene as a new approach for the synthesis of porous superparamagnetic and ferromagnetic composite*

microspheres of narrow size distribution. Journal of Materials Chemistry, 2011. **21**(39): p. 15764-15772.

46. Maity, D., et al., *Synthesis of magnetite nanoparticles via a solvent-free thermal decomposition route.* Journal of Magnetism and Magnetic Materials, 2009. **321**(9): p. 1256-1259.

47. Wu, W., Q. He, and C. Jiang, *Magnetic iron oxide nanoparticles: synthesis and surface functionalization strategies.* Nanoscale research letters, 2008. **3**(11): p. 397.

48. Giri, S., et al., *Magnetic properties of α- Fe_2O_3 nanoparticle synthesized by a new hydrothermal method.* Journal of Magnetism and Magnetic Materials, 2005. **285**(1-2): p. 296-302.

49. Hu, X., J.C. Yu, and J. Gong, *Fast production of self-assembled hierarchical α- Fe_2O_3 nanoarchitectures.* The Journal of Physical Chemistry C, 2007. **111**(30): p. 11180-11185.

50. Jing, Z. and S. Wu, *Synthesis and characterization of monodisperse hematite nanoparticles modified by surfactants via hydrothermal approach.* Materials Letters, 2004. **58**(27-28): p. 3637-3640.

51. Liu, X., et al., *Hydrothermal synthesis and characterization of α-FeOOH and α- Fe_2O_3 uniform nanocrystallines.* Journal of alloys and compounds, 2007. **433**(1-2): p. 216-220.

52. Laudise, R., *Hydrothermal synthesis of crystals 50 Years Progress in Crystal Growth: A Reprint Collection*. 2004, Amsterdam: Elsevier) p.

53. Chen, Y., et al., *Synthesis of porous hollow Fe 3 O 4 beads and their applications in lithium ion batteries.* Journal of Materials Chemistry, 2012. **22**(11): p. 5006-5012.

54. Hu, P., et al., *Fabrication of monodisperse magnetite hollow spheres.* The Journal of Physical Chemistry C, 2008. **113**(3): p. 900-906.

55. Lin, X., et al., *Formation mechanism and magnetic properties of hollow Fe_3O_4 nanospheres synthesized without any surfactant.* CrystEngComm, 2012. **14**(24): p. 8658-8663.

56. You, L.-J., et al., *Ultrafast hydrothermal synthesis of high quality magnetic core phenol–formaldehyde shell composite microspheres using the microwave method.* Langmuir, 2012. **28**(28): p. 10565-10572.

57. Cheng, X.-L., et al., *Liquid–liquid interface-assisted solvothermal synthesis of durian-like α- Fe_3O_4 hollow spheres constructed by nano-polyhedrons.* CrystEngComm, 2012. **14**(9): p. 3056-3062.

58. Gao, G., et al., *Solvothermal synthesis and characterization of size-controlled monodisperse Fe_3O_4 nanoparticles.* Journal of materials science, 2010. **45**(13): p. 3483-3489.

59. Sun, X., et al., *Size-controlled synthesis of magnetite (Fe_3O_4) nanoparticles coated with glucose and gluconic acid from a single Fe (III) precursor by a sucrose bifunctional hydrothermal method.* The Journal of Physical Chemistry C, 2009. **113**(36): p. 16002-16008.

60. Xu, J.-S. and Y.-J. Zhu, *α- Fe_2O_3 hierarchically hollow microspheres self-assembled with nanosheets: surfactant-free solvothermal synthesis, magnetic and photocatalytic properties.* CrystEngComm, 2011. **13**(16): p. 5162-5169.

61. Xu, H., B.W. Zeiger, and K.S. Suslick, *Sonochemical synthesis of nanomaterials.* Chemical Society Reviews, 2013. **42**(7): p. 2555-2567.

62. Bang, J.H. and K.S. Suslick, *Applications of ultrasound to the synthesis of nanostructured materials.* Advanced materials, 2010. **22**(10): p. 1039-1059.

63. Suslick, K.S., *Sonochemistry.* science, 1990. **247**(4949): p. 1439-1445.

64. Abu-Much, R. and A. Gedanken, *Sonochemical synthesis under a magnetic field: structuring magnetite nanoparticles and the destabilization of a colloidal magnetic aqueous solution under a magnetic field.* The Journal of Physical Chemistry C, 2008. **112**(1): p. 35-42.

65. Morel, A.-L., et al., *Sonochemical approach to the synthesis of Fe_3O_4@ SiO2 core−shell nanoparticles with tunable properties.* Acs Nano, 2008. **2**(5): p. 847-856.

66. Mukh-Qasem, R.A. and A. Gedanken, *Sonochemical synthesis of stable hydrosol of Fe_3O_4 nanoparticles.* Journal of colloid and interface science, 2005. **284**(2): p. 489-494.

67. Wu, W., et al., *Sonochemical synthesis, structure and magnetic properties of air-stable Fe_3O_4/Au nanoparticles.* Nanotechnology, 2007. **18**(14): p. 145609.

68. Zhang, S., et al., *Sonochemical formation of iron oxide nanoparticles in ionic liquids for magnetic liquid marble.* Physical Chemistry Chemical Physics, 2012. **14**(15): p. 5132-5138.

69. Yew, Y.P., et al., *Green synthesis of magnetite (Fe_3O_4) nanoparticles using seaweed (Kappaphycus alvarezii) extract.* Nanoscale research letters, 2016. **11**(1): p. 276.

70. Shahwan, T., et al., *Green synthesis of iron nanoparticles and their application as a Fenton-like catalyst for the degradation of aqueous cationic and anionic dyes.* Chemical Engineering Journal, 2011. **172**(1): p. 258-266.

71. Silveira, C., et al., *Iron-oxide nanoparticles by the green synthesis method using Moringa oleifera leaf extract for fluoride removal.* Environmental technology, 2017: p. 1-11.

72. Kanagasubbulakshmi, S. and K. Kadirvelu, *Green Synthesis of Iron Oxide Nanoparticles using Lagenaria Siceraria and Evaluation of its Antimicrobial Activity.* Defence Life Science Journal, 2017. **2**(4): p. 422-427.

73. Mahdavi, M., et al., *Green biosynthesis and characterization of magnetic iron oxide (Fe_3O_4) nanoparticles using seaweed (Sargassum muticum) aqueous extract.* Molecules, 2013. **18**(5): p. 5954-5964.

74. Saranya, S., K. Vijayarani, and S. Pavithra, *Green Synthesis of Iron Nanoparticles using Aqueous Extract of Musa ornata Flower Sheath against Pathogenic Bacteria.* Indian Journal of Pharmaceutical Sciences, 2017. **79**(5): p. 688-694.

75. El-Kassas, H.Y., M.A. Aly-Eldeen, and S.M. Gharib, *Green synthesis of iron oxide (Fe_3O_4) nanoparticles using two selected brown seaweeds: characterization and application for lead bioremediation.* Acta Oceanologica Sinica, 2016. **35**(8): p. 89-98.

76. Venkateswarlu, S., et al., *Biogenic synthesis of Fe_3O_4 magnetic nanoparticles using plantain peel extract.* Materials Letters, 2013. **100**: p. 241-244.

77. Senapati, S., et al., *Extracellular biosynthesis of bimetallic Au–Ag alloy nanoparticles.* Small, 2005. **1**(5): p. 517-520.

78. Klaus, T., et al., *Silver-based crystalline nanoparticles, microbially fabricated.* Proceedings of the National Academy of Sciences, 1999. **96**(24): p. 13611-13614.

79. Bansal, V., et al., *Biosynthesis of zirconia nanoparticles using the fungus Fusarium oxysporum.* Journal of Materials Chemistry, 2004. **14**(22): p. 3303-3305.

80. Duan, H., D. Wang, and Y. Li, *Green chemistry for nanoparticle synthesis.* Chemical Society Reviews, 2015. **44**(16): p. 5778-5792.

81. El-Kassas, H.Y. and M.M. El-Sheekh, *Cytotoxic activity of biosynthesized gold nanoparticles with an extract of the red seaweed Corallina officinalis on the MCF-7 human breast cancer cell line.* Asian Pac J Cancer Prev, 2014. **15**(15): p. 4311-4317.

82. Sathishkumar, M., K. Sneha, and Y.-S. Yun, *Immobilization of silver nanoparticles synthesized using Curcuma longa tuber powder and extract on cotton cloth for bactericidal activity.* Bioresource technology, 2010. **101**(20): p. 7958-7965.

83. Makarov, V., et al., *"Green" nanotechnologies: synthesis of metal nanoparticles using plants.* Acta Naturae (англоязычная версия), 2014. **6**(1 (20)).

84. Sintubin, L., W. Verstraete, and N. Boon, *Biologically produced nanosilver: current state and future perspectives.* Biotechnology and Bioengineering, 2012. **109**(10): p. 2422-2436.

85. Mukherjee, S., et al., *Green chemistry approach for the synthesis and stabilization of biocompatible gold nanoparticles and their potential applications in cancer therapy.* Nanotechnology, 2012. **23**(45): p. 455103.

86. Baker, S., et al., *Plants: emerging as nanofactories towards facile route in synthesis of nanoparticles.* BioImpacts: BI, 2013. **3**(3): p. 111.

87. Díaz-Gómez, J.L., et al., *Anti-Cancer Activity of Maize Bioactive Peptides.* Frontiers in chemistry, 2017. **5**: p. 44.

88. Chaturvedi, N., et al., *Cereals nutraceuticals, health ennoblement and diseases obviation: a comprehensive review.* J. Appl. Pharm. Sci, 2011. **1**(7): p. 6-12.

89. Li, J.-T., et al., *Apoptosis in human hepatoma HepG2 cells induced by corn peptides and its anti-tumor efficacy in H22 tumor bearing mice.* Food and chemical toxicology, 2013. **51**: p. 297-305.

90. Ortiz-Martinez, M., et al., *Antiproliferative effect of peptide fractions isolated from a quality protein maize, a white hybrid maize, and their derived peptides on hepatocarcinoma human HepG2 cells.* Journal of Functional Foods, 2017. **34**: p. 36-48.

91. de Mejia, E., et al., *Bioavailability and safety of food peptides*. 2012: CRC Press: Boca Raton, FL.

92. Xue, Z., et al., *Effect of rapeseed peptide on DNA damage and apoptosis in Hela cells.* Experimental and Toxicologic Pathology, 2010. **62**(5): p. 519-523.

93. Hernandez-Ledesma, B., C.-C. Hsieh, and O. Ben, *Lunasin, a novel seed peptide for cancer prevention.* Peptides, 2009. **30**(2): p. 426-430.

94. Nadumane, V.K. and B. Timsina, *Anti-cancer potential of banana flower extract: An in vitro study.* Bangladesh Journal of Pharmacology, 2014. **9**(4): p. 628-635.

95. Asuquo, E.G. and C.E. Udobi, *Antibacterial and toxicity studies of the ethanol extract of Musa paradisiaca leaf.* Cogent Biology, 2016. **2**(1): p. 1219248.

96. Mahmoudi, M., et al., *Superparamagnetic iron oxide nanoparticles (SPIONs): development, surface modification and applications in chemotherapy.* Advanced drug delivery reviews, 2011. **63**(1-2): p. 24-46.

97. Institute, N.C. *What Is Cancer?* [cited 2018 June 22]; Available from: https://www.cancer.gov/about-cancer/understanding/what-is-cancer.

98. Institute, N.C. *Common Cancer Types*. [cited 2018 June 22]; Available from: https://www.cancer.gov/types/common-cancers.

99. Institute, N.C. *Types of Cancer Treatment*. [cited 2018 June 22]; Available from: https://www.cancer.gov/about-cancer/treatment/types.

100. Society, A.C. *Types of Cancer Treatment*. [cited 2018 June 22]; Available from: https://www.cancer.org/treatment/treatments-and-side-effects/treatment-types.html.

101. Hsu, Y.-L., et al., *Acacetin-induced cell cycle arrest and apoptosis in human non-small cell lung cancer A549 cells.* Cancer letters, 2004. **212**(1): p. 53-60.

102. Manasanch, E.E. and R.Z. Orlowski, *Proteasome inhibitors in cancer therapy.* Nature Reviews Clinical Oncology, 2017. **14**(7): p. 417.

103. Almond, J. and G. Cohen, *The proteasome: a novel target for cancer chemotherapy.* Leukemia, 2002. **16**(4): p. 433.

104. Frankland-Searby, S. and S.R. Bhaumik, *The 26S proteasome complex: an attractive target for cancer therapy.* Biochimica et Biophysica Acta (BBA)-Reviews on Cancer, 2012. **1825**(1): p. 64-76.

105. McConkey, D.J. and K. Zhu, *Mechanisms of proteasome inhibitor action and resistance in cancer.* Drug Resistance Updates, 2008. **11**(4-5): p. 164-179.

106. Crawford, L.J., B. Walker, and A.E. Irvine, *Proteasome inhibitors in cancer therapy.* Journal of cell communication and signaling, 2011. **5**(2): p. 101-110.

107. Zhao, J., et al., *Facile surfactant-free synthesis and characterization of Fe_3O_4@ 3-aminophenol–formaldehyde core–shell magnetic microspheres.* Journal of Materials Chemistry A, 2015. **3**(2): p. 519-524.

108. Wang, J. and J. Yi, *Cancer cell killing via ROS: to increase or decrease, that is the question.* Cancer biology & therapy, 2008. **7**(12): p. 1875-1884.

109. Biology-pages. *Excitable Cells*. [cited 2018 12/10/2018]; Available from: http://www.biology-pages.info/E/ExcitableCells.html.

110. Donath, M.Y. and S.E. Shoelson, *Type 2 diabetes as an inflammatory disease.* Nature Reviews Immunology, 2011. **11**(2): p. 98.

111. Lang, F., et al., *Ion channels in cell proliferation and apoptotic cell death.* The Journal of membrane biology, 2005. **205**(3): p. 147-157.

112. Razik, M.A. and J.A. Cidlowski, *Molecular interplay between ion channels and the regulation of apoptosis.* Biological research, 2002. **35**(2): p. 203-207.

113. Jean-Yves, L.G., et al., *Voltage-gated ion channels, new targets in anti-cancer research.* Recent patents on anti-cancer drug discovery, 2007. **2**(3): p. 189-202.

114. Roger, S., et al., *Voltage-gated sodium channels: new targets in cancer therapy?* Current pharmaceutical design, 2006. **12**(28): p. 3681-3695.

115. Kunzelmann, K., *Ion channels and cancer.* The Journal of membrane biology, 2005. **205**(3): p. 159.

116. Prevarskaya, N., et al., *Ion channels in death and differentiation of prostate cancer cells.* Cell death and differentiation, 2007. **14**(7): p. 1295.

117. Rao, V.R., et al., *Voltage-gated ion channels in cancer cell proliferation.* Cancers, 2015. **7**(2): p. 849-875.

118. Bronstein-Sitton, P.D., *Noemi;".* Ion Channels in Cancer." Modulator (Spring 2003): p. 1-7.

119. Yang, M. and W.J. Brackenbury, *Membrane potential and cancer progression.* Frontiers in physiology, 2013. **4**: p. 185.

120. Academy, K. *Q & A: Neuron depolarization, hyperpolarization, and action potentials*. [cited 2018 12/10/2018]; Available from: https://www.khanacademy.org/science/biology/human-biology/neuron-nervous-system/a/depolarization-hyperpolarization-and-action-potentials.

121. Bortner, C.D., F.M. Hughes, and J.A. Cidlowski, *A primary role for K+ and Na+ efflux in the activation of apoptosis.* Journal of Biological Chemistry, 1997. **272**(51): p. 32436-32442.

122. Kerr, J.F., A.H. Wyllie, and A.R. Currie, *Apoptosis: a basic biological phenomenon with wideranging implications in tissue kinetics.* British journal of cancer, 1972. **26**(4): p. 239.

123. Wyllie, A.H., *Glucocorticoid-induced thymocyte apoptosis is associated with endogenous endonuclease activation.* Nature, 1980. **284**(5756): p. 555.

124. Rahman, S.S.U., et al., *Single step growth of iron oxide nanoparticles and their use as glucose biosensor.* Results in physics, 2017. **7**: p. 4451-4456.

125. Basavegowda, N., K. Mishra, and Y.R. Lee, *Sonochemically synthesized ferromagnetic Fe_3O_4 nanoparticles as a recyclable catalyst for the preparation of pyrrolo [3, 4-c] quinoline-1, 3-dione derivatives.* RSC Advances, 2014. **4**(106): p. 61660-61666.

126. Njagi, E.C., et al., *Biosynthesis of iron and silver nanoparticles at room temperature using aqueous sorghum bran extracts.* Langmuir, 2010. **27**(1): p. 264-271.

127. Nadagouda, M.N., et al., *In vitro biocompatibility of nanoscale zerovalent iron particles (NZVI) synthesized using tea polyphenols.* Green Chemistry, 2010. **12**(1): p. 114-122.

128. Senapati), R.G.K.K. *How does the addition of a base cause Fe_3O_4 to precipitate in coprecipitation?* 2014 [cited 2018 15/10/2018]; Available from: https://www.researchgate.net/post/How_does_the_addition_of_a_base_cause_Fe3O4_to_precipitate_in_coprecipitation.

129. Carter, N., *Physical Properties of Iron Oxide Nanoparticles.* 2015.

130. Awwad, A.M. and N.M. Salem, *A green and facile approach for synthesis of magnetite nanoparticles.* Nanoscience and Nanotechnology, 2012. **2**(6): p. 208-213.

131. Balamurughan, M., et al., *Ocimum sanctum leaf extract mediated green synthesis of iron oxide nanoparticles: spectroscopic and microscopic studies.* Journal of Chemical and Pharmaceutical Sciences ISSN, 2014. **974**: p. 2115.